S-acylation stabilizes ligand-induced receptor kinase complex formation during plant pattern-triggered immune signalling.

Charlotte H. Hurst[1,2], Dionne Turnbull[1], Kaltra Xhelilaj[3], Sally Myles[1], Robin L. Pflughaupt[4], Michaela Kopischke[5], Paul Davies[4], Susan Jones[6], Silke Robatzek[5,7], Cyril Zipfel[5,8], Julien Gronnier[3,8], Piers A. Hemsley[1,2*]

Affiliations:

[1] Division of Plant Sciences, School of Life Sciences, University of Dundee, Dow Street, Dundee, DD1 5EH, Scotland, UK.

[2] Cell and Molecular Sciences, The James Hutton Institute, Invergowrie, Dundee, DD2 5DA, Scotland, UK.

[3] ZMBP Universität Tübingen, Auf der Morgenstelle 32, D-72076 Tübingen, DE

[4] Medical Research Council Protein Phosphorylation and Ubiquitylation Unit, School of Life Sciences, University of Dundee, Dow Street, Dundee, DD1 5EH, Scotland, UK.

[5] The Sainsbury Laboratory, University of East Anglia, Norwich Research Park, NR4 7UH, Norwich, England, UK.

[6] Information and Computational Sciences, The James Hutton Institute, Invergowrie, Dundee, DD2 5DA, Scotland, UK.

[7] Present address - LMU Munich Biocenter, Großhadener Strasse 4, 82152 Planegg, DE.

[8] Institute of Plant and Microbial Biology, Zurich-Basel Plant Science Center, University of Zurich, 8008 Zurich, CH.

* Correspondence: p.a.hemsley@dundee.ac.uk

Summary

Plant receptor kinases are key transducers of extracellular stimuli, such as the presence of beneficial or pathogenic microbes or secreted signalling molecules. Receptor kinases are regulated by numerous post-translational modifications. Here, using the immune receptor kinases FLS2 and EFR, we show that S-acylation at a cysteine conserved in all plant receptor kinases is crucial for function. S-acylation involves the addition of long-chain fatty acids to cysteine residues within proteins, altering their biophysical properties and behaviour within the membrane environment. We observe S-acylation of FLS2 at C-terminal kinase domain cysteine residues within minutes following perception of its ligand flg22, in a BAK1 co-receptor dependent manner. We demonstrate that S-acylation is essential for FLS2-mediated immune signalling and resistance to bacterial infection. Similarly, mutating the corresponding conserved cysteine residue in EFR supressed elf18 triggered signalling. Analysis of unstimulated and activated FLS2-containing complexes using microscopy, detergents and native membrane DIBMA nanodiscs indicates that S-acylation stabilises and promotes retention of activated receptor kinase complexes at the plasma membrane to increase signalling efficiency.

Key words

S-acylation; palmitoylation; receptor-kinase; receptor-like kinase; FLS2; EFR; microdomain; nanodomain; plasma membrane; Arabidopsis

Introduction

The plasma membrane defines the boundary between the cell interior and the external environment. Receptor kinases (RKs) found in the plasma membrane act as the principle means of perception for most of the stimuli that a plant encounters, such as hormones, signalling peptides and microbe associated molecular patterns (MAMPs). RKs comprise the largest single gene family in plants [1, 2] and are central to current efforts to breed or engineer crops able to withstand emerging pathogen threats, interact with beneficial microbes or better tolerate abiotic stress [3-6]. Understanding the mechanisms and principles underlying the formation and activation of RK complexes is therefore critical to informing these approaches.

The RK FLAGELLIN SENSING 2 (FLS2) is the receptor for bacterial flagellin and the flagellin-derived peptide flg22 [7], and is an archetype for RK research, particularly in the area of host-microbe interactions. flg22 binding to the extracellular leucine-rich repeats of FLS2 induces interaction with the co-receptor BAK1/SERK3 (BRI1-ASSOCIATED RECEPTOR KINASE 1/SOMATIC EMBRYOGENESIS RECEPTOR-LIKE KINASE 3). Subsequent transphosphorylation of FLS2 by BAK1 initiates a cascade of immune signalling to activate anti-bacterial defence responses. As part of this overall process, flg22 perception leads to changes in FLS2 phosphorylation [8], SUMOylation [9] and ubiquitination [10] state, indicating a high degree of post-translational regulation. FLS2 activation also alters overall complex composition [7, 9-18] and physical properties [19]. However, the underlying mechanisms and functional relevance of these changes remain unknown.

S-acylation is a reversible post-translational modification, whereby long chain fatty acids are added to cysteine residues by protein S-acyl transferases [20] and removed by acyl-protein thioesterases [21]. This modification can lead to changes in protein trafficking, stability, and turnover. S-acylation has been proposed to drive membrane phase partitioning [22, 23] while changes in protein S-acylation state have been hypothesised to modulate protein-protein and protein-membrane interactions, or even alter protein activation states [24], direct experimental evidence to support these ideas is lacking. We recently discovered that FLS2, alongside all other plant RKs tested, is post-translationally modified by S-acylation [25]. Here we demonstrate that ligand induced S-acylation of FLS2 and EFR RKs, at a site conserved in all RKs across the span of plant evolutionary history, acts as a positive regulator of signal transduction. Mechanistically, ligand-induced S-acylation of FLS2 promotes stability and retention of receptor complexes at the plasma membrane.

Results

FLS2 undergoes ligand responsive S-acylation.

Our previous analysis of FLS2 identified the juxta-transmembrane (TM) domain cysteines (Cys830,831) as being constitutively S-acylated, but this modification was dispensable for FLS2 function [25]. All RK superfamily members subsequently tested, with or without a juxta-TM S-acylation site homologous to FLS2 $C^{830,831}$, also appear to be S-acylated [25]. This indicates that non-juxta-TM S-acylation sites, potentially conserved in all RKs, exist. Other post-translational modifications affecting FLS2, and the broader RK superfamily, including phosphorylation [26], ubiquitination [10] and SUMOylation [9] are all responsive to ligand binding. Given the dynamic nature of S-acylation [21] we were interested to determine whether FLS2 S-acylation state is also ligand responsive. In Col-0 wild type plants, FLS2 S-acylation significantly increased above basal levels in controls following 20-min exposure to the FLS2 agonist peptide flg22. FLS2 S-acylation subsequently returned to basal levels within 1 h (figures 1A and 1B). Consistent with its ligand-dependency, FLS2 S-acylation was contingent upon the FLS2 co-receptor BAK1 (BRI1-ASSOCIATED KINASE) (figure 1C). PUB12/13 (PLANT U-BOX12/13) are ubiquitin ligases proposed to promote FLS2 endocytosis and attenuate signalling [10]. FLS2 S-acylation is impaired in the *pub12/13* double mutant, suggesting that PUB12/13 action may be required for S-acylation to occur. Additionally, flg22 induced S-acylation of FLS2 was unaffected in *chc2-1* (CLATHRIN HEAVY CHAIN 2) mutants [17] of clathrin heavy chain 2 (figure 1C). These data indicate that FLS2 S-acylation occurs after initiation of FLS2 signalling and the hypothesised ubiquitination thought to mark FLS2 for internalisation, but before endocytosis of FLS2 occurs. Treatment of Arabidopsis Col-0 plants with elf18, an immunogenic peptide derived from bacterial elongation factor Tu, recognised by the RK EFR (ELONGATION FACTOR-Tu RECEPTOR) that acts similarly to FLS2 [27], failed to elevate FLS2 S-acylation (figure 1D). This demonstrates that the increase in FLS2 S-acylation is specifically linked to activation of FLS2 signalling and not a general phenomenon related to activation of RK-mediated defence responses.

flg22 responsive S-acylation sites of FLS2 are located in the kinase domain C-terminus and are conserved across the wider plant receptor kinase superfamily.

107 FLS2 $C^{830,831}S$ mutants [25] lacking the juxta-TM S-acylation retain the ability to be S-acylated in
108 response to flg22 (figure S1A, 5 and 20 minute timepoints). FLS2 therefore contains S-acylation
109 sites in addition to $C^{830,831}$ that are responsive to ligand perception. While FLS2 $C^{830,831}S$ expressed
110 at native levels in unstimulated Arabidopsis is very weakly S-acylated [25] (figure S1A, untreated),
111 we observed S-acylation of FLS2 $C^{830,831}S$ in the absence of flg22 when overexpressed in *Nicotiana*
112 *benthamiana*. Mutation of FLS2 Cys 1132 and 1135 in addition to Cys 830 and 831 (FLS2
113 $C^{830,831,1132,1135}S$) abolished FLS2 S-acylation compared to FLS2 $C^{830,831}S$ (figure S1B) when
114 overexpressed in *N. benthamiana*, suggesting that Cys1132/1135 are sites of S-acylation.
115 Following this observation, we found that *fls2c/proFLS2:FLS2* $C^{1132,1135}S$ Arabidopsis plants (figure
116 S1C) showed no increase in S-acylation following flg22 treatment (figure 1E), indicating that these
117 cysteines are the sites of ligand inducible S-acylation. Interestingly, 1-2 conserved cysteine
118 residues at the C-terminus of the kinase domain corresponding to FLS2 Cys 1132 and/or 1135, are
119 found across all RKs in Arabidopsis and RKs from Charophycean algae (figure S2) at the base of
120 the broader Streptophyte lineage with high quality genome assemblies [28], suggesting a
121 evolutionarily conserved and important role for these cysteines. In support of this hypothesis, we
122 found that EFR-GFP [29] transiently expressed in *N. benthamiana* undergoes an elf18-induced
123 increase in S-acylation, and this is blocked by mutation of the EFR Cys 975, the cysteine
124 homologous to flg22 responsive FLS2 Cys 1135 (figure S1D, S1E, S2).
125
126 **Receptor kinase C-terminal S-acylation is required for early immune signalling**
127 Consistent with the evolutionarily conserved nature of the FLS2 kinase domain S-acylated
128 cysteines amongst RKs, mutation of these cysteines affects FLS2 function. *fls2c/proFLS2:FLS2*
129 $C^{1132,1135}S$ plants are impaired in several aspects of early immune signalling, such as reactive
130 oxygen species production, MAP kinase activation and immune gene expression (figure 2A, B, C).
131 In the absence of flg22 ligand, both FLS2-3xMyc-GFP and FLS2 $C^{1132,1135}S$-3xMyc-GFP show similar
132 accumulation at the plasma membrane (figure S3A; water treatments) and similar lateral
133 membrane mobility (figure S3B, C; water treatments). Remorins are plasma membrane resident
134 proteins that form clusters and have been proposed as markers for membrane nanodomains [30].
135 Specifically, REM1.3 (Remorin 1.3) nanodomains have previously been shown to have strong
136 spatial overlap with FLS2 nanodomains [31]. Both FLS2-3xMyc-GFP and FLS2 $C^{1132,1135}S$-3xMyc-
137 GFP show similar co-localization with REM1.3 nanodomains (figure S3D, E, F). These data
138 combined indicate that there is no aberrant basal cellular behaviour of the FLS2 $C^{1132,1135}S$ mutant
139 when compared to FLS2 that could account for the observed reduction in response to flg22. To
140 determine whether the conserved C-terminal cysteines may have a general role in RK function,
141 we transiently expressed EFR-GFP [29] and EFR $C^{975}S$-GFP in *N. benthamiana.* We observed that
142 elf18-induced MAP kinase phosphorylation and immune gene induction was reduced in EFR $C^{975}S$-
143 GFP expressing plants compared to EFR-GFP (figure 2D, E). This demonstrates that mutation of
144 the conserved C-terminal cysteine in both FLS2 and EFR has a similar effect on early outputs and
145 indicates a conserved mode of action. Structural homology modelling of FLS2 indicates that the
146 $C^{1132,1135}S$ mutation does not affect FLS2 kinase domain structure (figure S4). Kinase activity is also
147 dispensable for activation of signalling by EFR [32]. The observed effects of the FLS2 $C^{1132,1135}S$ and

148 EFR $C^{975}S$ mutations on early signalling therefore cannot be readily explained through deleterious
149 effects on kinase activity or structure.
150
151 **FLS2 kinase domain S-acylation is required for late immune responses and anti-bacterial**
152 **immunity**
153 Early signalling outputs resulting from bacterial perception by FLS2 lead to longer term sustained
154 responses to promote immunity. In line with decreased early immune responses, later flg22-
155 induced gene expression and physiological outputs, such as *PR1* (PATHOGENESIS-RELATED GENE
156 1) expression and seedling growth inhibition, were affected in *fls2c/proFLS2:FLS2* $C^{1132,1135}S$ plants
157 (figure 3A, B). As a result of these cumulative signalling defects, FLS2 $C^{1132,1135}S$ failed to
158 complement the hyper-susceptibility of *fls2* mutant plants to the pathogenic bacterium
159 *Pseudomonas syringae* pv. tomato (*Pto*) DC3000 (figure 3C).
160
161 **S-acylation of FLS2 stabilizes flg22-induced FLS2-BAK1 signalling complexes within the plasma**
162 **membrane**
163 Differential solubility in cold non-ionic detergents such as Triton X-100 or IGEPAL CA-630, leading
164 to formation of detergent soluble or resistant membrane fractions (DSM and DRM respectively),
165 has been used to characterise overall changes to protein physical properties, particularly in the
166 context of protein S-acylation [19, 33]. *fls2c/proFLS2:FLS2* and *fls2c/proFLS2:FLS2* $C^{1132,1135}S$ plants
167 were treated with or without flg22 and total cold IGEPAL CA-630 protein extracts were separated
168 into DRM and DSM/cytosol fractions [34]. Following flg22 treatment, FLS2 abundance in cold
169 IGEPAL CA-630 derived DRMs showed a slight reduction, while FLS2 $C^{1132,1135}S$ DRM abundance
170 decreased by ~50% (figure 4A, B). Overall, these data suggest a change in protein and/or lipid
171 environment of the FLS2 $C^{1132,1135}S$ containing complex compared to wild type within 20 minutes
172 of flg22 exposure.
173
174 Assessment of flg22-induced FLS2-BAK1 complex formation by co-immunoprecipitation following
175 solubilisation with cold IGEPAL CA-630 [35] indicated that the observed FLS2-BAK1 interaction
176 was reduced in FLS2 $C^{1132,1135}S$ mutants (figure 4C). Furthermore, flg22-induced BAK1 S^{612} auto-
177 phosphorylation [36], used as a marker of *in vivo* complex formation, was also weaker in FLS2
178 $C^{1132,1135}S$-expressing plants (figure 4C), supporting these biochemical observations. In contrast to
179 IGEPAL CA-630, diisobutylene/maleic acid (DIBMA) copolymer does not form DRM-like fractions.
180 DIBMA disrupts lipid-lipid, but not protein-protein or protein-lipid, interactions to form
181 membrane nanodiscs containing protein complexes within their membrane environment [37]. Co-
182 immunoprecipitation of DIBMA-solubilised FLS2-BAK1 and FLS2 $C^{1132,1135}S$-BAK1 complexes after
183 20 minutes of flg22 treatment (figure 4C) indicates that FLS2-BAK1 interactions are likely stabilized
184 by protein-protein and protein-lipid interactions that are reduced or absent from FLS2 $C^{1132,1135}S$-
185 BAK1 complexes.
186
187 Examination of FLS2 mobility by VA-TIRF microscopy (figure S3B, C) shows no detectable change
188 in FLS2-3xMyc-GFP or FLS2 $C^{1132,1135}S$-3xMyc-GFP motion within the plasma membrane following
189 flg22 treatment. However, we observed a decrease in the number of particles of FLS2 $C^{1132,1135}S$-

190 3xMyc-GFP, but not wild type FLS2-3xMyc-GFP, at the plasma membrane following 20 minutes of
191 flg22 treatment (figure S3B, C), suggesting premature or accelerated endocytosis of flg22 bound
192 FLS2 $C^{1132,1135}$S-3xMyc-GFP. Altogether, our observations indicate that FLS2 S-acylation stabilises
193 FLS2-BAK1 association and maintains FLS2 in an signalling competent state at the plasma
194 membrane.
195
196 **Discussion**
197 FLS2, a prototypical RK, has been previously shown to be S-acylated at a pair of juxta-
198 transmembrane domain cysteines (Cys 830,831), but S-acylation at these sites is apparently
199 dispensable for function [25]. Here we demonstrate that FLS2 is S-acylated at additional cysteine
200 residues (Cys 1132,1135) in a ligand-responsive manner and that this is required for efficient
201 flg22-triggered signalling and resistance to *P. syringae* DC3000 bacterial infection. FLS2 S-acylation
202 occurs within minutes of flg22 perception and requires the co-receptor BAK1 and the PUB12/13
203 ubiquitin ligases, but does not require CHC2 function (figure 1). We therefore propose that FLS2
204 S-acylation occurs as a result of FLS2 activation but precedes entry into the endocytic pathway.
205 Supporting this hypothesis, preventing ligand mediated FLS2 S-acylation from occurring by using
206 *fls2c/proFLS2:FLS2* $C^{1132,1135}S$ plants reduces early signalling outputs, such as the phosphorylation
207 of MAPK and the production of ROS (figure 2), processes unimpaired in mutants affecting FLS2
208 endocytosis [15, 17]. Indeed, our data (figure S3B, S3C) suggests a model where FLS2 S-acylation
209 delays endocytosis and stabilises the FLS2-BAK1 complex at the plasma membrane, thereby
210 helping to sustain signalling competence. This failure to sufficiently prolong signalling competence
211 also explains the defects observed in *fls2c/proFLS2:FLS2* $C^{1132,1135}S$ plants where subsequent
212 signalling outputs such as *PR1* induction, growth inhibition and, ultimately, resistance to
213 pathogenic bacteria (figure 3) are greatly impaired. Following activation, FLS2 is endocytosed and
214 degraded, with new FLS2 being synthesised within approximately 1 hour of initial flg22 perception
215 [38, 39]. Our observation that FLS2 S-acylation returns to near basal levels after 1 hour correlates
216 with reported timings of degradation and *de-novo* FLS2 synthesis [38] but, at present, we cannot
217 exclude an active process of FLS2 de-S-acylation prior to endocytosis.
218
219 Sequence analysis of RKs from across the Streptophyte lineages indicate that the S-acylation site
220 identified here at the C-terminus of the FLS2 kinase domain is conserved across plant RK families
221 throughout evolutionary history (figure S2). Assessment of the elongation factor-Tu perceiving
222 receptor kinase EFR indicates that, similarly to FLS2, it undergoes ligand responsive S-acylation at
223 this conserved cysteine (Cys 975). Mutation of this cysteine in EFR recapitulates the downstream
224 signalling defects observed in S-acylation defective FLS2. We therefore hypothesise that there is
225 a conserved role for S-acylation at these sites in other plant RKs. Recently, the
226 P2K1/DORN1/LecRK-I.9 RK was proposed to undergo de-S-acylation followed by re-S-acylation
227 during immune responses [40]. However, the site proposed is unique to the LecRK family, being
228 distinct in proposed function, location, sequence, and structure to the universally conserved
229 cysteine identified here that is also present in P2K1 but was not considered in the previous work.
230 These data demonstrate that, in common with other post-translational modifications, S-acylation
231 may affect multiple sites within an RK with differing effects on RK function (e.g. this work and

232 [25]). The position and effect of the S-acylation site identified here at the C-terminus of the FLS2
233 and EFR kinase domains is highly conserved amongst plant RKs, and is also found in the closely
234 related receptor-like cytoplasmic kinases (RLCKs) that act downstream of activated RKs. This
235 opens up the exciting possibility that S-acylation at the conserved C-terminal kinase site may
236 potentially regulate the function of all RKs (and RLCKs) across plants in a similar manner to FLS2
237 and EFR. However, this hypothesis awaits further empirical testing.
238
239 RK signalling is initiated by binding of a ligand (e.g., flg22) to its receptor (e.g., FLS2), which then
240 facilitates the binding of a co-receptor (e.g., BAK1/SERK3). While this constitutes the minimal
241 ligand recognition complex, substantial evidence supports a far larger number of proteins being
242 intimately associated with both unstimulated and activated receptors and co-receptors. Indeed,
243 existing data indicates that during the process of activation RKs recruit or eject specific proteins
244 from their complexes [13, 18, 41, 42], but precise molecular mechanisms determining these
245 changes are not known. Live cell imaging of unstimulated FLS2 and BAK1 indicates that presence
246 or absence of the RK FERONIA (FER), has marked effects on nanoscale organisation and mobility
247 of RKs in the plasma membrane. In addition, activation of the RK FERONIA (FER) by its ligand
248 RALF23 alters BAK1 organisation and mobility [43]. This indicates that both complex composition,
249 and the activation state of individual components, affects behaviour of the whole complex.
250 Changes in direct protein-protein interaction can be explained by allosteric effects. However, it is
251 also possible that alteration of the immediate (annular) lipid environment composition, curvature,
252 or structure, brought about by changes in the physical properties of the complex, would act to
253 recruit or exclude proteins based on their solubility and packing in the membrane environment
254 surrounding the complex. This is, in essence, one of the principles proposed to underlie the
255 formation of membrane nanodomains [44, 45]. Activation of FLS2 following flg22 perception has
256 been reported to decrease overall plasma membrane fluidity and increase plasma membrane
257 order [46], while changing sterol abundance in the plasma membrane affects all stages of FLS2
258 signalling [47]. This indicates that membrane composition and structure have profound effects on
259 receptor complex function and supports the principle of protein-lipid interactions affecting or
260 effecting RK function. S-acylation, being a fatty acid-based modification of proteins, has been
261 shown to affect protein physical character and behaviour in membrane environments [33, 48]. S-
262 acylation also affects membrane micro-curvature [23], a key theoretical determinant of
263 membrane component partitioning required for nanodomain formation [44]. We therefore
264 hypothesise that FLS2 S-acylation modulates interactions between FLS2 and immune complex
265 components and/or FLS2 proximal membrane lipid components and may effect changes in the
266 composition of both. Altogether our data supports a model where flg22-induced, BAK1-
267 dependent FLS2 S-acylation sustains FLS2-BAK1 association, prevents premature internalisation
268 of activated FLS2 complex and, overall, acts to promote immune signalling.
269
270 **Acknowledgments**
271 We would like to thank Antje Heese and Paul Birch for critical discussions and advice during the
272 preparation of this manuscript. Ari Sadanandom provided *P. syringae* pv. tomato DC3000. *bak1-*
273 *4* seed was provided by Delphine Chinchilla, *chc2-1* seed by Antje Heese and *pub12/13* seed by

Libo Shan. This work was supported by BBSRC EASTBIO-DTP studentship (grant number BB/M010996/1) to SM and PH, BBSRC grants BB/M024911/1 and BB/P007902/1 to PH, Royal Society Grant RG140531 to PH, a Heisenberg fellowship from the Deutsche Forschungsgemeinschaft to SR, the Gatsby Charitable Foundation, the University of Zürich, the European Research Council (Grant Agreement 773153 IMMUNO-PEPTALK) to CZ, the European Molecular Biology Organization (EMBO Long-Term Fellowship 438-2018), and the German Research Foundation (DFG grant CRC1101-A09) to JG. SJ was supported by the Scottish Government's Rural and Environment Science and Analytical Services division (RESAS).

Author Contributions:

CRediT statement

CHH: Conceptualization, Methodology, Validation, Formal analysis (Equal), Investigation (Lead), Data curation (Equal), Writing - Review & Editing, Visualization. **DT**: Methodology, Validation, Investigation (Equal), Writing - Review & Editing. **SM**: Validation, Investigation. **MK**: Investigation. **SJ**: Methodology, Software, Investigation. **KX**: Investigation, Formal analysis (Equal). **SR**: Resources, Writing - Review & Editing, Supervision, Funding acquisition (Equal). **CZ**: Resources, Writing - Review & Editing, Supervision, Funding acquisition (Equal). **JG**: Methodology, Formal analysis (Equal), Investigation (Equal), Data curation (Equal), Writing - Review & Editing, Supervision, Visualization, Funding acquisition (Equal). **PAH**: Conceptualization (Lead), Methodology (Lead), Validation, Formal analysis (Lead), Investigation, Data curation (Equal), Resources, Writing - Original Draft (Lead), Writing - Review & Editing (Lead), Visualization (Lead), Supervision (Lead), Project administration (Lead), Funding acquisition (Equal).

Competing Interest Statement: No competing interests declared.

Figure Legends

Figure 1. FLS2 S-acylation increases upon flg22 perception. A. Representative western blot of FLS2 S-acylation state in Arabidopsis Col-0 plants treated with 1 μM flg22 peptide or water as determined by acyl-biotin exchange assay. EX - indicates S-acylation state, LC - loading control, Hyd - indicates presence (+) or absence (-) of hydroxylamine. **B.** Quantification of western blot data in A. showing change in S-acylation state in Arabidopsis Col-0 plants treated with 1 μM flg22 (green) or water (orange). S-acylation state is shown relative to untreated plants (black dashed line). n = 3 biological repeats. Box plot shows median and IQR, whiskers indicate data points within 1.5 x IQR. Significance of difference between flg22 and water treatments at each timepoint was determined by ANOVA and Tukey's HSD test. **C.** S-acylation of FLS2 in response to flg22 requires BAK1 and PUB12/13 but not CHC2. S-acylation state was determined by acyl-biotin exchange after 20 minutes exposure to 1 μM flg22 and is shown relative to untreated Arabidopsis plants of the same genotype (dashed line). Box plot shows median and IQR, whiskers indicate data points within 1.5 x IQR. Significant differences of each genotype to flg22 treated Arabidopsis Col-0 as determined by Student's t-test are shown. **D.** FLS2 undergoes S-acylation in response to flg22 treatment but not elf18. S-acylation state as determined by acyl-biotin exchange after 20 minutes of treatment using 1 μM peptide or water is shown relative to untreated Arabidopsis plants (black,

316 dashed line). Box plot shows median and IQR, whiskers indicate data points within 1.5 x IQR.
317 Significant differences of elf18 or water treatment compared to flg22 treated Arabidopsis Col-0
318 as determined by Student's t-test are shown. **E.** FLS2 $C^{1132,1135}S$ mutants are blocked in flg22
319 mediated increases in S-acylation. S-acylation state is shown following 20 minutes 1 μM flg22
320 treatment relative to untreated Arabidopsis plants of the same genotype (black, dashed line).
321 Box plot shows median and IQR, whiskers indicate data points within 1.5 x IQR. Significant
322 difference of each line compared to flg22 treated Col-0 as determined by Student's t-test are
323 shown.
324
325 **Figure 2. Acute responses to bacterial elicitor perception are reduced in FLS2 $C^{1132,1135}S$ and EFR-**
326 **$C^{975}S$ expressing plants. A.** ROS production induced by 100 nM flg22 treatment of Arabidopsis
327 seedlings. Data points are the sum of the 3 highest consecutive readings per sample. n = 10 per
328 genotype. Statistical outliers are shown as open circles. Box shows median and IQR, whiskers
329 show +/- 1.5 x IQR. Statistically significant differences at $p < 0.01$ are indicated (a, b) and were
330 calculated using ANOVA and Tukey HSD tests. **B.** MAPK activation in *fls2/FLS2pro:FLS2* $C^{1132,1135}S$
331 Arabidopsis seedlings in response to 100 nM flg22 as determined over time by immunoblot
332 analysis. pMAPK6/pMAPK3 show levels of active form of each MAPK. MAPK6 indicates total levels
333 of MAPK6 as a loading control. Upper shadow band in MAPK6 blot is RuBisCO detected non-
334 specifically by secondary antibody. **C.** *WRKY40* mRNA abundance after 1 hour treatment with 1
335 μM flg22 in fls2/FLS2pro:FLS2 $C^{1132,1135}S$ Arabidopsis seedlings as determined by qRT-PCR. Values
336 were calculated using the ΔΔCT method, error bars represent RQMIN and RQMAX and constitute
337 the acceptable error level for a 95% confidence interval according to Student's t-test. **D.**
338 *NbACRE31* mRNA abundance after 3 hour treatment with 1 μM elf18 in EFR-GFP and EFR $C^{975}S$-
339 GFP expressing *N. benthamiana* plants as determined by qRT-PCR. Values were calculated using
340 the ΔΔCT method, error bars represent RQMIN and RQMAX and constitute the acceptable error
341 level for a 95% confidence interval according to Student's t-test. **E.** MAPK activation in EFR-GFP
342 and EFR $C^{975}S$-GFP expressing *N. benthamiana* plants in response to 15 minutes treatment with 1
343 μM elf18 as determined by immunoblot analysis. pSIPK/pWIPK show levels of active form of each
344 MAPK. WIPK indicates total levels of WIPK as a loading control. EFR-GFP and EFR $C^{975}S$-GFP levels
345 are shown as a control for dosage effects on MAPK activation.
346
347 **Figure 3. FLS2 S-acylation is required for long term immune response outputs. A.** Induction of
348 *PR1* gene expression after 24 hours treatment with 1 mM flg22 in *fls2/FLS2pro:FLS2* $C^{1132,1135}S$
349 seedlings as determined by qRT-PCR. Values were calculated using the $\Delta\Delta_{CT}$ method, error bars
350 represent RQMIN and RQMAX and constitute the acceptable error level for a 95% confidence
351 interval according to Student's t-test. Significant differences in transcript mRNA detected in
352 *fls2/FLS2pro:FLS2* $C^{1132,1135}S$ Arabidopsis seedlings compared to Col-0 levels in flg22 treated
353 samples are indicated. Similar data were obtained over 3 biological repeats. **B.** Inhibition of
354 growth after 10 days of 1 μM flg22 treatment is reduced in *fls2/FLS2pro:FLS2* $C^{1132,1135}S$
355 Arabidopsis seedlings. Box and whisker plots show data from 7 biological repeats (box denotes
356 median and IQR, whiskers show +/- 1.5 x IQR), significant differences at $p < 0.01$ are indicated (a,

357 b, c) and calculated by ANOVA with Tukey HSD test. **C.** Resistance to *P. syringae* pv. tomato
358 DC3000 infection is impaired by loss of FLS2 S-acylation in *fls2/FLS2pro:FLS2* $C^{1132,1135}S$ Arabidopsis
359 plants. Box and whisker plots show data from 7 biological repeats (box denotes median and IQR,
360 whiskers show +/- 1.5 x IQR, outliers are shown as open circles), significant differences at $p < 0.05$
361 are indicated (a, b, c) and calculated by ANOVA with Tukey HSD test.
362
363 **Figure 4. FLS2 $C^{1132,1135}S$ shows reduced interaction with BAK1 following flg22 stimulation. A.**
364 FLS2 $C^{1132,1135}S$ shown altered DRM partitioning compared to FLS2. Arabidopsis flg22 treated
365 seedlings were lysed in cold IGEPAL CA-630 buffer and separated into detergent soluble (S) and
366 detergent resistant (R) fractions. Relative partitioning of FLS2 into each fraction was determined
367 by western blotting with anti-FLS2 rabbit polyclonal antibody. Purity of fractions is shown by
368 western blot using anti-PM H+ ATPase (PM ATPase, DRM marker), anti-Calnexin1/2 (CNX1/2, DSM
369 marker) and anti-UDP-glucose pyrophosphorylase (UGPase, cytosol marker) antibodies. **B.**
370 Quantification of FLS2 data shown in A from 3 biological repeats. Box plot shows median and IQR,
371 whiskers indicate data points within 1.5 x IQR. Significance was calculated using Student's t-test.
372 **C.** FLS2 was immunoprecipitated from IGEPAL CA-630 (left) or DIBMA (right) solubilised flg22
373 treated Arabidopsis seedling lysates using anti-FLS2 rabbit polyclonal antibody. BAK1 recovery
374 was assessed using rabbit polyclonal anti-BAK1 antibody. flg22 induced BAK1
375 autophosphorylation at Ser612 was assessed in IGEPAL CA-630 solubilised input samples using
376 rabbit polyclonal anti-BAK1 pS612 antibody.
377
378 **Materials and Methods**
379 **Cloning and constructs**
380 All *FLS2* mutant variants used in this study are based on fully functional $FLS2_{pro}$*:FLS2* construct able
381 to complement *fls2* mutants [49] containing the described FLS2 promoter and open reading frame
382 with stop codon [50]. All construct manipulations were performed on pENTR D-TOPO based
383 vectors. Nucleotide changes were generated using Q5 site directed mutagenesis kit (NEB)
384 according to the manufacturer's guidelines. $FLS2_{pro}$*:FLS2-3xMYC-EGFP* and $FLS2_{pro}$*:FLS2* $C^{1132,1135}S$-
385 *3xMYC-EGFP* were made by recombinatorial cloning in yeast using a 3xMYC-EGFP PCR fragment
386 amplified from $FLS2_{pro}$*:FLS2-3xMYC-EGFP* [39] recombined with pENTR D-TOPO $FLS2_{pro}$*:FLS2* or
387 pENTR D-TOPO $FLS2_{pro}$*:FLS2* $C^{1132,1135}S$. Entry clones were recombined into pK7WG,0 [51] using
388 Gateway technology (ThermoFisher) to generate expression constructs. Expression constructs
389 were transformed into *Agrobacterium tumefaciens* strain GV3101 pMP90 [52] for transformation
390 of either Arabidopsis or *Nicotiana benthamiana*.
391
392 **Plant lines and growth conditions**
393 All Arabidopsis lines were in the Col-0 accession background. The *fls2* [50], *bak1-4* [53], pub12/13
394 [10] and *chc2-1* [17] mutants have all been described previously. Transgenic *fls2/*$FLS2_{pro}$*:FLS2* are
395 already described [49] and *fls2/*$FLS2_{pro}$*:FLS2* $C^{1132,1135}S$ mutant variant lines were generated by
396 Agrobacterium-mediated floral dip transformation [54]. T_3 homozygous plants were used for all
397 experiments. Plant material for experiments was grown on 0.5x MS medium, 0.8% phytagar under
398 16:8 light:dark cycles at 20 °C in MLR-350 growth chambers (Panasonic). For transient expression

399 *Nicotiana benthamiana* plants were grown in 16:8 light:dark cycles at 24 °C and used at 4-5 weeks
400 old. *A. tumefaciens* mediated transient expression was performed as described [55] using an
401 OD600 of 0.1 of each expression construct alongside the p19 silencing suppressor at an OD600 of
402 0.1. Tissue was harvested 48-60 hours post infiltration.
403
404 **Eliciting peptides**
405 Flg22 peptide (QRLSTGSRINSAKDDAAGLQIA) was synthesised by Dundee Cell Products (Dundee,
406 UK). Elf18 peptide (Ac-SKEKFERTKPHVNVGTIG) was synthesised by Peptide Protein Research Ltd.
407 (Bishops Waltham, UK).
408
409 **Seedling growth inhibition**
410 For each biological replicate four days post-germination, 10 seedlings of the named genotypes
411 were transferred to 12-well plates (5 seedlings per well), ensuring the cotyledons were not
412 submerged. Wells contained 2 mL of 0.5x MS liquid medium with or without 1 µM flg22. Seedlings
413 were incubated for 10 days and the fresh weight of pooled seedlings in each genotype for each
414 treatment measured and an average taken. Flg22- treated/untreated weights for each genotype
415 were calculated and presented data is an average of these data over three biological repeats. Fully
416 independent biological repeats were performed over a period of 6 months with each genotype
417 only being present once in each repeat.
418
419 **MAPK activation**
420 Essentially as for [56]; 6 Arabidopsis seedlings of each genotype 10 days post germination were
421 treated with 100 nM flg22 for the indicated times in 2 mL 0.5x MS medium. The 6 seedlings from
422 each genotype at each time point for each treatment were pooled before further analysis. Fully
423 independent biological repeats were performed over a period of 2 years with each genotype only
424 being present once in each repeat. To assess EFR induced MAPK activation in *N. benthamiana*
425 leaves from 5-week-old plants were transiently transformed by agrobacterium infiltration (OD600
426 0.1 of each construct plus p19 at OD600 0.1). 60 hours after transformation, 1 µM elf18 peptide
427 in water or water only was infiltrated into the leaf and samples harvested after 15 minutes.
428 Samples were subsequently processed as described [56].
429
430 **Reactive oxygen species production**
431 Protocol based on Mersmann et al. (2010). Essentially, 10 seedlings of each genotype were grown
432 for 14 days in 100 µL of 0.5x MS medium with 0.5% sucrose, in 96-well plates (PerkinElmer).
433 Conditions were maintained at 22 °C with 12:12 light:dark cycles. Growth medium was exchanged
434 for water with 10 nM flg22 for 1 hour, before replacing with water for a further 1 hour. ROS burst
435 was then induced by replacing with a solution containing 100 nM flg22, 400 nM luminol (Fluka),
436 and 20 µg/mL peroxidase (Sigma). Luminescence in each well was measured every 2 minutes in a
437 Varioskan Lux (Thermo Fisher) for 30 cycles (approx. 1 hour total).
438
439 **Gene expression analysis**

440 Ten seedlings of each genotype 10 days post-germination were treated with 1 µM flg22 or water
441 for the indicated times. The 10 seedlings from each genotype/treatment at each time point for
442 each treatment were pooled before further analysis. RNA was extracted using RNAeasy Plant kit
443 with on column DNAse digestion according to the manufacturer's instructions (Qiagen). Two
444 micrograms RNA was reverse transcribed using a High-Capacity cDNA Reverse Transcription kit
445 (Applied Biosystems). All transcripts were amplified using validated gene-specific primers [49].
446 Expression levels were normalized against *PEX4* (At5g25760) [57]. Each sample was analyses in
447 triplicate (technical repeats) for each primer pair within each biological repeat. Relative
448 quantification (RQ) was achieved using the $\Delta\Delta_{CT}$ (comparative cycle threshold) method [58].
449 Significant differences between samples were determined from a 95% confidence interval
450 calculated using the t-distribution. Fully independent biological repeats were performed over a
451 period of 2 years with each genotype only being present once in each repeat.
452
453 **Bacterial infection assays**
454 Infection assays of Arabidopsis lines by *Pseudomonas syringae* pv. tomato DC3000 were
455 performed using seedling flood inoculation assays as described [59].
456
457 **Western blotting**
458 FLS2 was detected using rabbit polyclonal antisera raised against the C-terminus of FLS2 as
459 previously described [12, 60]. Anti-p44/42 MAPK (Erk1/2) (Cell Signalling Technology #9102) was
460 used to detect phosphorylated MAPK3/6 according to manufacturer's recommendations at
461 1:2000 dilution. Total Arabidopsis MAPK6 or *N. benthamiana* WIPK was detected using anti-
462 Arabidopsis MPK6 (Sigma A7104) at 1:2000. Rabbit polyclonal antibodies against BAK1 were as
463 described [35] or obtained from Agrisera (AS12 1858) and used at 1:5000 dilution. BAK1 phospho-
464 S612 was detected using polyclonal rabbit antisera as described [36]. Plasma membrane H+
465 ATPase (Agrisra AS13 2671), Calnexin 1/2 (Agrisera AS12 2365) and UDP-glucose
466 pyrophosphorylase (Agrisera AS05 086) were all used at 1:2500. HRP (ECL) or fluorophore (Licor
467 CLx) conjugated secondary antibodies were used to visualise antibody reacting proteins, and
468 Clean-Blot HRP (Thermo Fisher) secondary antibody was used for immunoprecipitation
469 experiments. ECL Western blots were developed using SuperSignal West pico and femto in a 3:1
470 ratio by volume and signal captured using a Syngene G:box storm imager and quantitative photon
471 count data stored as Syngene SGD files. Signal intensity was quantified from SGD files using
472 Syngene GeneTools software. Fluorescent western blots were imaged using a Licor CLx controlled
473 by ImageStudio and quantified using Licor ImageStudio.
474
475 **S-acylation assays**
476 S-acylation assays using acyl-biotin exchange (ABE) were performed exactly as described [60]. For
477 flg22-dependent changes in FLS2 S-acylation, 7 seedlings 10 days post germination were
478 transferred to each well of 12-well plates. Each well contained 2 mL 0.5 x MS liquid medium.
479 Seedling were incubated for 24 hours on an orbital mixer (Luckham R100/TW Rotatest Shaker, 38
480 mm orbit at 75 RPM). Thereafter, 100 µL of 0.5 x MS media containing flg22 was added to give a
481 final flg22 concentration of 10 µM. Seedlings were incubated with continued mixing for the

482 indicated times before harvesting. Relative S-acylation is calculated using: (EX+ intensity$^{SAMPLE\ X}$ /
483 LC+ intensity$^{SAMPLE\ X}$) / (EX+ intensity$^{REFERENCE\ SAMPLE}$ / LC+ intensity $^{REFERENCE\ SAMPLE}$) [61]. Sample X
484 refers to the sample of interest, reference sample is typically untreated control plants.
485
486 **Co-immunoprecipitation assays using IGEPAL CA-630**
487 Seedlings grown on solid 0.5x MS for 30-35 days were transferred to wells of a 6-well plates and
488 grown for 7 days in 0.5x MS 2 mM MES-KOH, pH 5.8. Thereafter, the seedlings were transferred
489 in beakers containing 40 mL of 0.5x MS 2 mM MES-KOH, pH 5.8 and subsequently treated with
490 sterile mQ water with or without flg22 (final concentration of 100 nM) and incubated for 10
491 minutes. The seedlings were then frozen in liquid nitrogen and proteins extracted in 50 mM Tris-
492 HCl pH 7.5, 150 mM NaCl, 10% glycerol, 5 mM dithiothreitol, 1% protease inhibitor cocktail (Sigma
493 Aldrich), 2 mM Na_2MoO_4, 2.5 mM NaF, 1.5 mM activated Na_3VO_4, 1 mM phenylmethanesulfonyl
494 fluoride and 0.5% IGEPAL for 40 minutes at 4 °C. Lysates were clarified at 10,000 g for 20 minutes
495 at 4 °C and the supernatants were filtered through miracloth. For immunoprecipitations, α-rabbit
496 Trueblot agarose beads (eBioscience) coupled with α-FLS2 antibodies [11] were incubated with
497 the crude extract for 3 hours at 4 °C. Subsequently, beads were washed 3 times (50 mM Tris-HCl
498 pH 7.5, 150 mM NaCl, 1 mM phenylmethanesulfonyl fluoride, 0.1% IGEPAL) before adding
499 Laemmli buffer and incubating for 10 minutes at 95 °C. Protein samples were separated in 10%
500 bisacrylamide gels at 150 V for approximately 2 hours and transferred into activated PVDF
501 membranes at 100 V for 90 minutes. Immunoblotting was performed with antibodies diluted in
502 blocking solution (5% fat-free milk in TBS with 0.1% (v/v) Tween-20). Antibodies used in this study:
503 α-BAK1 [35] (1:5000); α-FLS2 [11] (1:1000); α-BAK1 pS612 [36] (1:3000). Blots were developed
504 with Pierce ECL/ ECL Femto Western Blotting Substrate (Thermo Scientific). The following
505 secondary antibodies were used: anti-rabbit IgG-HRP Trueblot (Rockland, 18-8816-31, dilution
506 1:10000) for detection of FLS2-BAK1 co-immunoprecipitation or anti-rabbit IgG (whole molecule)–
507 HRP (A0545, Sigma, dilution 1:10000) for all other western blots.
508
509 **Co-immunoprecipitation assays using Diisobutylene-maleic acid (DIBMA)**
510 For each genotype, 2 x 10 seedlings 10 days post-germination were transferred to each well of
511 12-well plate containing 2 mL 0.5 x MS liquid medium and incubated for 24 hours on an orbital
512 mixer (Luckham R100/TW Rotatest Shaker, 38 mm orbit at 75 RPM). Thereafter, 100 µL of 0.5 x
513 MS media containing flg22 was added to give a final flg22 concentration of 10 µM. The seedlings
514 were further incubated with continued mixing for 20 minutes prior to harvesting and blotting dry.
515 Tissue was lysed in 500 µl of lysis buffer (50 mM Tris-HCl pH 7.2, 10% v/v glycerol, 150 mM NaCl,
516 1% w/v DIBMA (Anatrace BMA101), with protease inhibitors (1% v/v, Sigma P9599)) and
517 incubated at room temperature for 1 hour with gentle end-over-end mixing. The lysate was
518 centrifuged at 5,000 g for 1 minute and the supernatant filtered through 2 layers of miracloth and
519 combined with an additional 500 µl of filtered lysis buffer (without DIMBA). The clarified lysate
520 was further centrifuged at 16,000 g for 1 minute and the supernatant applied to Amicon 0.5 mL
521 100 kDa MWCO spin filtration columns and centrifuged at 14,000 g until the retentate was <50
522 µl. The retentate was diluted to 500 µl with IP buffer (50 mM Tris-HCl pH 7.2, 10% glycerol, 200

523 mM L-arginine, with protease inhibitor (0.5% v/v, Sigma P9599) and centrifuged at 14,000 g until
524 the retentate was <50 μl. The spin column was inverted and eluted into a 1.5 mL microfuge tube
525 by centrifugation at 100 g for 1 minute The eluate was diluted to 500 μl with IP buffer, of which
526 20 μl was retained as an input control. Magnetic protein A beads (20 μl per IP reaction) were
527 coated with 5 μg αFLS2 antibody overnight at 4 °C. The resulting beads were washed for 5 minutes
528 with IP buffer containing 0.5 M NaCl followed by 2 washes with IP buffer and resuspended in IP
529 buffer to 100 μl per IP reaction. The resulting FLS2-coated magnetic protein A beads were added
530 to the DIBMA solubilised protein solution and incubated for 3 hours at room temperature with
531 end-over-end mixing. Thereafter, the beads were washed three times with IP buffer, resuspended
532 in 30 μl 2x LDS sample buffer with 2-mercaptoethanol and incubated at 65 °C for 5 minutes with
533 shaking at 1000 RPM. The samples were separated on a 7.5% SDS-PAGE gel prior to transfer to
534 PVDF and western blotting.
535
536 **Detergent resistant membrane preparation**
537 To evaluate flg22-dependent changes in FLS2 detergent resistant membrane occupancy, 7
538 seedlings 10 days post-germination were transferred to each well of a 12-well plate, of which each
539 well contained 2 mL 0.5 x MS liquid medium. Seedlings were incubated for 24 hours on an orbital
540 mixer (Luckham R100/TW Rotatest Shaker, 38 mm orbit at 75 RPM), after which 100 µL of 0.5 x
541 MS media containing flg22 was added to give a final flg22 concentration of 10 µM. The seedlings
542 were further incubated with continuous mixing as before for 20 minutes before harvesting and
543 snap freezing in liquid nitrogen. All subsequent steps were performed at 4 °C or on ice. The
544 seedlings were then lysed in 0.5 mL ice cold 1% (v/v) IGEPAL CA-630 in 25 mM Tris-HCl pH 7.4,
545 150 mM NaCl, 2 mM EDTA, and 0.1% (v/v) protease inhibitors (Sigma-Aldrich, P9599). Lysates
546 were clarified at 500 g and filtered through 1 layer of miracloth. The filtrate was centrifuged at
547 16,000 g for 30 minutes and the supernatant retained as a detergent soluble fraction (DSM) and
548 mixed 3:1 with 4x reducing (2-mercaptoethanol) LDS sample buffer. The detergent resistant pellet
549 (DRM) was gently washed with 1 mL lysis buffer, centrifuged at 16,000 g for 5 minutes, and the
550 supernatant discarded. The resulting pellet was resuspended in 27 µL of 3:1 lysis buffer: 4x
551 reducing LDS sample buffer, after which 25 µL of the DRM and DSM were separated by 7.5% SDS-
552 PAGE and probed using anti-FLS2 polyclonal antibody as described [60]. Presence of PM H+
553 ATPase (DRM enriched), Calnexin 1/2 (DSM enriched) [62] and UDP-glucose pyrophosphorylase
554 (cytosol) [63] were used as markers for DRM purity.
555
556 **Variable Angle - Total Internal Reflection Fluorescence (VA-TIRF) microscopy**
557 VA-TIRF microscopy was performed using an inverted Leica GSD equipped with a 160x objective
558 (NA = 1.43, oil immersion), and an Andor iXon Ultra 897 EMCCD camera. Images were acquired
559 by illuminating samples with a 488 nm solid state diode laser, a cube filter with an excitation filter
560 488/10 and an emission filter 535/50 for FLS2-GFP, and a 532 nm solid state diode laser, a cube
561 filter with an excitation filter 532/10 and an emission filter 600/100 for mRFP-REM1.3. Optimum
562 critical angle was determined as giving the best signal-to-noise.
563

564 **Single particle tracking analysis**
565 *Nicotiana benthamiana* plants (14-21 days old) were infiltrated with *Agrobacterium tumefaciens*
566 (strain GV3101) solution of OD_{600} = 0.5 and imaged 24 to 30 hours post infiltration. Image
567 acquisition was done within 2 to 20 min after 1 µM flg22 or corresponding mock treatment. For
568 single particle tracking experiments, image time series were recorded at 5 frames per second (0.2
569 s exposure time) by VA-TIRFM. Analyses were carried out as previously described [64], using the
570 plugin TrackMate7 [65] in Fiji [66]. Single particles were segmented frame-by-frame by applying
571 a Laplacian of Gaussian filter and estimated particle size of 0.3 µm. Individual single particle were
572 localized with sub-pixel resolution using a built-in quadratic fitting scheme. Single particle
573 trajectories were reconstructed using a simple linear assignment problem [67] with a maximal
574 linking distance of 0.2 µm and without gap-closing. Only tracks with at least seven successive
575 points (tracked for 1.4 s) were selected for further analysis. Diffusion coefficients of individual
576 particles were extracted using SPTAnalysis [68] based on cosine filtered and maximum likelihood
577 estimates analysis of particles displacement.
578
579 **Co-localization analyses**
580 *Nicotiana benthamiana* plants (14-21 days old) were infiltrated with *Agrobacterium tumefaciens*
581 (strain GV3101) solution of OD = 0.2 and imaged 48 hours post infiltration. Images were recorded
582 by VA-TIRFM using 250 ms exposure time. As previously reported [31], we emphasised cluster
583 formation in the presented images by using the 'LoG3D' plugin [69]. Quantitative co-localization
584 analyses of the FLS2-GFP and mRFP-REM1.3 were carried out as previously described [31], with
585 minor modification. Using FiJi, images were subjected to a background subtraction using the
586 "Rolling ball" method (radius = 20 pixels) and smoothed. We selected regions of TIRF micrographs
587 with homogeneous illumination for both FLS2-GFP and mRFP-REM1.3. The Pearson co-localization
588 coefficients were assessed using the JACoP plugin of FIJI [70]. For comparison, we determined
589 values of correlation, which could be observed by chance by calculating the Pearson coefficient
590 after flipping one of the two images.
591
592 **Structural modelling of FLS2 kinase domain**
593 The FLS2 intracellular domain (amino acids 831-1173) was submitted to the Phyre2 [71] server
594 (http://www.sbg.bio.ic.ac.uk/phyre2/) in default settings. The solved BIR2 kinase domain
595 structure (PDB 4L68, residues 272-600) [72] was identified as the best match and FLS2 residues
596 841-1171 were successfully modelled onto the BIR2 structure (confidence 100%, coverage 89%).
597 Cys to Ser mutational effects were modelled using Missense3D [73] in default settings.
598
599 **Supplemental figure Legends**
600 **Supplemental figure 1. A.** FLS2 $C^{830,831}S$ stably expressed in Arabidopsis *fls2* null mutant
601 background retains the ability to be weakly S-acylated following flg22 treatment. S-acylation state
602 was determined by acyl-biotin exchange assay. EX - indicates S-acylation state, LC - loading
603 control, Hyd - indicates presence (+) or absence (-) of hydroxylamine. **B.** Mutation of FLS2
604 Cys1132,1135 to serine abolishes residual S-acylation observed in FLS2 $C^{830,831}S$ when over-
605 expressed in *Nicotiana benthamiana*. EX - indicates S-acylation state, LC - loading control, Hyd -

606 indicates presence (+) or absence (-) of hydroxylamine. **C.** Expression levels of FLS2 $C^{1132,1135}S$ in
607 *fls2/FLS2pro:FLS2 FLS2 $C^{1132,1135}S$* transgenic Arabidopsis lines used in this study. 50 mg total
608 protein from 7-day old seedlings was loaded per lane. MYH9.5 is a previously reported cross-
609 reacting protein with the primary anti-FLS2 antibody used . **D.** EFR-GFP expressed in *Nicotiana*
610 *benthamiana* undergoes S-acylation in a Cys975 dependant manner following 20 minutes of 1 μM
611 elf18 treatment when. S-acylation state was determined by determined by acyl-biotin exchange
612 assay. EX - indicates S-acylation state, LC - loading control, Hyd - indicates presence (+) or absence
613 (-) of hydroxylamine. **E.** Quantification of EFR S-acylation state shown in D. elf18 induced changes
614 to S-acylation state are shown relative to water treated (black dashed line). n = 3 biological
615 repeats. Box plot shows median and IQR, whiskers indicate data points within 1.5 x IQR.
616 Significance of difference between EFR and EFR $C^{975}S$ was determined by Student's t-test.
617
618 **Supplemental figure 2. Receptor Kinases contain a conserved C-terminal cysteine within the**
619 **kinase domain.** Alignment using at least one representative member from each of the wider
620 Arabidopsis RK superfamilies. Example receptor kinases found in *Chara braunii* (Cb) and
621 *Klebsormidium nitens* (Kn) with clear sub-family members in Arabidopsis are also included as
622 extant basal Streptophytes to illustrate evolutionary conservation of the proposed S-acylation
623 site. Uniprot IDs are given for *Chara* and *Klebsormidium* sequences. Alignment is centred on the
624 conserved $C[X]_7RP$ motif found in the loop between the G- and H-helices of the kinase domain.
625 Putative S-acylation site cysteines are highlighted in teal with the conserved +7 RP motif in orange.
626
627 **Supplemental figure 3. FLS2 S-acylation affects flg22 induced endocytosis but not unstimulated**
628 **basal behaviour. A.** FLS2-3xMyc-GFP and FLS2 $C^{1132,1135}S$-3xMyc-GFP accumulate similarly when
629 expressed in *N. benthamiana* in the absence of flg22, however, FLS2 $C^{1132,1135}S$-3xMyc-GFP is
630 cleared more rapidly than FLS2-3xMyc-GFP from the cell surface following flg22 exposure. Particle
631 counts per μm2 at the plasma membrane of single cells using TIRF microscopy. Box plot shows
632 median and IQR, whiskers indicate data points within 1.5 x IQR. FLS2-3xMyc-GFP mock n = 15 cells
633 and 15076 particles, FLS2-3xMyc-GFP flg22 treatment n = 19 cells and 14717 particles, FLS2
634 $C^{1132,1135}S$-3xMyc-GFP mock n = 12 cells and 12593 particles and FLS2 $C^{1132,1135}S$-3xMyc-GFP flg22
635 treatment n= 22 cells and 7468 particles. p values calculated by ANOVA and confidence groups at
636 $p < 0.05$ assigned using Tukey's HSD test. **B.** Representative images from single particle tracking
637 experiments of FLS2-3xMyc-GFP and FLS2 $C^{1132,1135}S$-3xMyc-GFP at the plasma membrane using
638 TIRF microscopy. Experiments performed transiently in *N. benthamiana*. **C.** Quantification of
639 average diffusion coefficient of single cells. Box plot shows median and IQR, whiskers indicate 1.5
640 x IQR. p values calculated by ANOVA and confidence groups at $p < 0.05$ assigned using Tukey's
641 HSD test. **D.** FLS2-3xMyc-GFP and FLS2 $C^{1132,1135}S$-3xMyc-GFP form nanodomains in the plasma
642 membrane and show similar co-localisation with mRFP-REM1.3 nanodomains when transiently
643 expressed in *N. benthamiana* in the absence of flg22. Representative micrographs of FLS2-3xMyc-
644 GFP and FLS2 $C^{1132,1135}S$-3xMyc-GFP (green) co-localisation with mRFP-REM1.3 (magenta) at the
645 plasma membrane of single epidermal cells using TIRF microscopy. **E.** Quantification of FLS2-
646 3xMyc-GFP or FLS2 $C^{1132,1135}S$-3xMyc-GFP co-localisation with mRFP-REM1.3 at the plasma
647 membrane of single epidermal cells. FLS2-3xMyc-GFP n = 14 cells, FLS2 $C^{1132,1135}S$-3xMyc-GFP n =

648 12 cells. Box plot shows median and IQR, whiskers indicate 1.5 x IQR. *p* value calculated using
649 Student's t-test. **F.** To determine whether measured co-localisation values shown in B (original)
650 were significant, co-localisation analysis was repeated after rotation of the mRFP-REM1.3 image
651 by 90 degrees (rotated). In all cases, co-localisation was reduced and overall significantly different,
652 indicating that the co-localisation observed in B is both specific and significant. *p* values were
653 calculated using Student's t-test.
654
655 **Supplemental figure 4. Mutation of kinase domain S-acylation site cysteines to serine in FLS2 is**
656 **not predicted to affect kinase domain structure. A.** Superimposition of the modelled structures
657 of FLS2 (white) and FLS2 $C^{1132,1135}S$ (blue) kinase domains. **B.** Zoomed in view of Cys1132,1135 in
658 FLS2 (yellow) and substituted serine (red) residues in FLS2 $C^{1132,1135}S$. Only the proton of Ser1132
659 is predicted to diverge from the FLS2 structure, being rotated by ~110 degrees compared to the
660 original cysteine. This rotation does not affect the position or packing of any other amino acid.
661
662 **References**

663 1. Shiu, S.H., and Bleecker, A.B. (2001). Receptor-like kinases from Arabidopsis form a
664 monophyletic gene family related to animal receptor kinases. PNAS *98*, 10763-10768.
665 2. Shiu, S.H., and Bleecker, A.B. (2003). Expansion of the receptor-like kinase/Pelle gene
666 family and receptor-like proteins in Arabidopsis. Plant Physiol *132*, 530-543.
667 3. Divi, U.K., and Krishna, P. (2009). Brassinosteroid: a biotechnological target for
668 enhancing crop yield and stress tolerance. N Biotechnol *26*, 131-136.
669 4. Lacombe, S., Rougon-Cardoso, A., Sherwood, E., Peeters, N., Dahlbeck, D., van Esse,
670 H.P., Smoker, M., Rallapalli, G., Thomma, B.P., Staskawicz, B., et al. (2010). Interfamily
671 transfer of a plant pattern-recognition receptor confers broad-spectrum bacterial
672 resistance. Nature biotechnology *28*, 365-369.
673 5. Gust, A.A., Brunner, F., and Nurnberger, T. (2010). Biotechnological concepts for
674 improving plant innate immunity. Curr Opin Biotechnol *21*, 204-210.
675 6. Marshall, A., Aalen, R.B., Audenaert, D., Beeckman, T., Broadley, M.R., Butenko, M.A.,
676 Cano-Delgado, A.I., de Vries, S., Dresselhaus, T., Felix, G., et al. (2012). Tackling drought
677 stress: receptor-like kinases present new approaches. Plant Cell *24*, 2262-2278.
678 7. Gomez-Gomez, L., and Boller, T. (2000). FLS2: an LRR receptor-like kinase involved in the
679 perception of the bacterial elicitor flagellin in Arabidopsis. Mol Cell *5*, 1003-1011.
680 8. Schulze, B., Mentzel, T., Jehle, A.K., Mueller, K., Beeler, S., Boller, T., Felix, G., and
681 Chinchilla, D. (2010). Rapid heteromerization and phosphorylation of ligand-activated
682 plant transmembrane receptors and their associated kinase BAK1. JBC *285*, 9444-9451.
683 9. Orosa, B., Yates, G., Verma, V., Srivastava, A.K., Srivastava, M., Campanaro, A., De Vega,
684 D., Fernandes, A., Zhang, C., Lee, J., et al. (2018). SUMO conjugation to the pattern
685 recognition receptor FLS2 triggers intracellular signalling in plant innate immunity.
686 NatComms *9*, 5185.
687 10. Lu, D., Lin, W., Gao, X., Wu, S., Cheng, C., Avila, J., Heese, A., Devarenne, T.P., He, P., and
688 Shan, L. (2011). Direct ubiquitination of pattern recognition receptor FLS2 attenuates
689 plant innate immunity. Science *332*, 1439-1442.
690 11. Chinchilla, D., Zipfel, C., Robatzek, S., Kemmerling, B., Nurnberger, T., Jones, J.D., Felix,
691 G., and Boller, T. (2007). A flagellin-induced complex of the receptor FLS2 and BAK1
692 initiates plant defence. Nature *448*, 497-500.

693 12. Heese, A., Hann, D.R., Gimenez-Ibanez, S., Jones, A.M., He, K., Li, J., Schroeder, J.I., Peck,
694 S.C., and Rathjen, J.P. (2007). The receptor-like kinase SERK3/BAK1 is a central regulator
695 of innate immunity in plants. PNAS *104*, 12217-12222.
696 13. Lu, D., Wu, S., Gao, X., Zhang, Y., Shan, L., and He, P. (2010). A receptor-like cytoplasmic
697 kinase, BIK1, associates with a flagellin receptor complex to initiate plant innate
698 immunity. PNAS *107*, 496-501.
699 14. Spallek, T., Beck, M., Ben Khaled, S., Salomon, S., Bourdais, G., Schellmann, S., and
700 Robatzek, S. (2013). ESCRT-I mediates FLS2 endosomal sorting and plant immunity. PLoS
701 Genet *9*, e1004035.
702 15. Smith, J.M., Leslie, M.E., Robinson, S.J., Korasick, D.A., Zhang, T., Backues, S.K., Cornish,
703 P.V., Koo, A.J., Bednarek, S.Y., and Heese, A. (2014). Loss of Arabidopsis thaliana
704 Dynamin-Related Protein 2B reveals separation of innate immune signaling pathways.
705 PLoS Pathog *10*, e1004578.
706 16. Kadota, Y., Sklenar, J., Derbyshire, P., Stransfeld, L., Asai, S., Ntoukakis, V., Jones, J.D.,
707 Shirasu, K., Menke, F., Jones, A., et al. (2014). Direct regulation of the NADPH oxidase
708 RBOHD by the PRR-associated kinase BIK1 during plant immunity. Mol Cell *54*, 43-55.
709 17. Mbengue, M., Bourdais, G., Gervasi, F., Beck, M., Zhou, J., Spallek, T., Bartels, S., Boller,
710 T., Ueda, T., Kuhn, H., et al. (2016). Clathrin-dependent endocytosis is required for
711 immunity mediated by pattern recognition receptor kinases. PNAS *113*, 11034-11039.
712 18. Stegmann, M., Monaghan, J., Smakowska-Luzan, E., Rovenich, H., Lehner, A., Holton, N.,
713 Belkhadir, Y., and Zipfel, C. (2017). The receptor kinase FER is a RALF-regulated scaffold
714 controlling plant immune signaling. Science *355*, 287-289.
715 19. Keinath, N.F., Kierszniowska, S., Lorek, J., Bourdais, G., Kessler, S.A., Asano, H.,
716 Grossniklaus, U., Schulze, W., Robatzek, S., and Panstruga, R. (2010). PAMP-induced
717 changes in plasma membrane compartmentalization reveal novel components of plant
718 immunity. JBC *285*, 39140-39149.
719 20. Hemsley, P.A., Kemp, A.C., and Grierson, C.S. (2005). The TIP GROWTH DEFECTIVE1 S-
720 acyl transferase regulates plant cell growth in Arabidopsis. Plant Cell *17*, 2554-2563.
721 21. Martin, B.R., Wang, C., Adibekian, A., Tully, S.E., and Cravatt, B.F. (2011). Global profiling
722 of dynamic protein palmitoylation. NatMet *9*, 84-89.
723 22. Hurst, C.H., and Hemsley, P.A. (2015). Current perspective on protein S-acylation in
724 plants: more than just a fatty anchor? Journal of Experimental Botany *66*, 1599-1606.
725 23. Mesquita, F.S., Abrami, L., Sergeeva, O., Turelli, P., Qing, E., Kunz, B., Raclot, C., Paz
726 Montoya, J., Abriata, L.A., Gallagher, T., et al. (2021). S-acylation controls SARS-CoV-2
727 membrane lipid organization and enhances infectivity. Dev Cell *56*, 2790-2807 e2798.
728 24. Turnbull, D., and Hemsley, P.A. (2017). Fats and function: protein lipid modifications in
729 plant cell signalling. Curr Opin Plant Biol *40*, 63-70.
730 25. Hurst, C.H., Wright, K.M., Turnbull, D., Leslie, K., Jones, S., and Hemsley, P.A. (2019).
731 Juxta-membrane S-acylation of plant receptor-like kinases is likely fortuitous and does
732 not necessarily impact upon function. Sci Rep *9*, 12818.
733 26. Wang, Y., Li, Z., Liu, D., Xu, J., Wei, X., Yan, L., Yang, C., Lou, Z., and Shui, W. (2014).
734 Assessment of BAK1 activity in different plant receptor-like kinase complexes by
735 quantitative profiling of phosphorylation patterns. J Proteomics *108*, 484-493.
736 27. Zipfel, C., Kunze, G., Chinchilla, D., Caniard, A., Jones, J.D., Boller, T., and Felix, G. (2006).
737 Perception of the bacterial PAMP EF-Tu by the receptor EFR restricts Agrobacterium-
738 mediated transformation. Cell *125*, 749-760.
739 28. Gong, Z., and Han, G.Z. (2021). Flourishing in water: the early evolution and
740 diversification of plant receptor-like kinases. PlantJ *106*, 174-184.

741 29. Holton, N., Nekrasov, V., Ronald, P.C., and Zipfel, C. (2015). The phylogenetically-related
742 pattern recognition receptors EFR and XA21 recruit similar immune signaling
743 components in monocots and dicots. PLoS Pathog *11*, e1004602.
744 30. Jarsch, I.K., Konrad, S.S., Stratil, T.F., Urbanus, S.L., Szymanski, W., Braun, P., Braun, K.H.,
745 and Ott, T. (2014). Plasma Membranes Are Subcompartmentalized into a Plethora of
746 Coexisting and Diverse Microdomains in Arabidopsis and Nicotiana benthamiana. Plant
747 Cell *26*, 1698-1711.
748 31. Bucherl, C.A., Jarsch, I.K., Schudoma, C., Segonzac, C., Mbengue, M., Robatzek, S.,
749 MacLean, D., Ott, T., and Zipfel, C. (2017). Plant immune and growth receptors share
750 common signalling components but localise to distinct plasma membrane nanodomains.
751 Elife *6*, e25114.
752 32. Bender, K.W., Couto, D., Kadota, Y., Macho, A.P., Sklenar, J., Bjornson, M., Petriello, A.,
753 Farre, M.F., Schwessinger, B., Ntoukakis, V., et al. (2021). ACTIVATION LOOP
754 PHOSPHORYLATION OF A NON-RD RECEPTOR KINASE INITIATES PLANT INNATE IMMUNE
755 SIGNALING. bioRxiv.
756 33. Abrami, L., Leppla, S.H., and van der Goot, F.G. (2006). Receptor palmitoylation and
757 ubiquitination regulate anthrax toxin endocytosis. J Cell Biol *172*, 309-320.
758 34. Brown, D.A. (2002). Isolation and use of rafts. Curr Protoc Immunol *Chapter 11*, Unit 11
759 10.
760 35. Roux, M., Schwessinger, B., Albrecht, C., Chinchilla, D., Jones, A., Holton, N., Malinovsky,
761 F.G., Tor, M., de Vries, S., and Zipfel, C. (2011). The Arabidopsis leucine-rich repeat
762 receptor-like kinases BAK1/SERK3 and BKK1/SERK4 are required for innate immunity to
763 hemibiotrophic and biotrophic pathogens. Plant Cell *23*, 2440-2455.
764 36. Perraki, A., DeFalco, T.A., Derbyshire, P., Avila, J., Sere, D., Sklenar, J., Qi, X., Stransfeld,
765 L., Schwessinger, B., Kadota, Y., et al. (2018). Phosphocode-dependent functional
766 dichotomy of a common co-receptor in plant signalling. Nature *561*, 248-252.
767 37. Oluwole, A.O., Danielczak, B., Meister, A., Babalola, J.O., Vargas, C., and Keller, S. (2017).
768 Solubilization of Membrane Proteins into Functional Lipid-Bilayer Nanodiscs Using a
769 Diisobutylene/Maleic Acid Copolymer. Angew Chem Int Ed Engl *56*, 1919-1924.
770 38. Smith, J.M., Salamango, D.J., Leslie, M.E., Collins, C.A., and Heese, A. (2014). Sensitivity
771 to Flg22 is modulated by ligand-induced degradation and de novo synthesis of the
772 endogenous flagellin-receptor FLAGELLIN-SENSING2. Plant Physiol *164*, 440-454.
773 39. Robatzek, S., Chinchilla, D., and Boller, T. (2006). Ligand-induced endocytosis of the
774 pattern recognition receptor FLS2 in Arabidopsis. Genes Dev *20*, 537-542.
775 40. Chen, D., Hao, F., Mu, H., Ahsan, N., Thelen, J.J., and Stacey, G. (2021). S-acylation of
776 P2K1 mediates extracellular ATP-induced immune signaling in Arabidopsis. NatComms
777 *12*, 2750.
778 41. Yeh, Y.H., Panzeri, D., Kadota, Y., Huang, Y.C., Huang, P.Y., Tao, C.N., Roux, M., Chien,
779 H.C., Chin, T.C., Chu, P.W., et al. (2016). The Arabidopsis Malectin-Like/LRR-RLK IOS1 is
780 Critical for BAK1-Dependent and BAK1-Independent Pattern-Triggered Immunity. Plant
781 Cell *28*, 1701-1721.
782 42. Imkampe, J., Halter, T., Huang, S., Schulze, S., Mazzotta, S., Schmidt, N., Manstretta, R.,
783 Postel, S., Wierzba, M., Yang, Y., et al. (2017). The Arabidopsis Leucine-Rich Repeat
784 Receptor Kinase BIR3 Negatively Regulates BAK1 Receptor Complex Formation and
785 Stabilizes BAK1. Plant Cell *29*, 2285-2303.
786 43. Gronnier, J., Franck, C.M., Stegmann, M., DeFalco, T.A., Abarca, A., von Arx, M., Dunser,
787 K., Lin, W., Yang, Z., Kleine-Vehn, J., et al. (2022). Regulation of immune receptor kinase

788 plasma membrane nanoscale organization by a plant peptide hormone and its
789 receptors. Elife *11*, e74162.
790 44. Allender, D.W., Giang, H., and Schick, M. (2020). Model Plasma Membrane Exhibits a
791 Microemulsion in Both Leaves Providing a Foundation for "Rafts". Biophys J *118*, 1019-
792 1031.
793 45. Mamode Cassim, A., Gouguet, P., Gronnier, J., Laurent, N., Germain, V., Grison, M.,
794 Boutte, Y., Gerbeau-Pissot, P., Simon-Plas, F., and Mongrand, S. (2019). Plant lipids: Key
795 players of plasma membrane organization and function. Prog Lipid Res *73*, 1-27.
796 46. Sandor, R., Der, C., Grosjean, K., Anca, I., Noirot, E., Leborgne-Castel, N., Lochman, J.,
797 Simon-Plas, F., and Gerbeau-Pissot, P. (2016). Plasma membrane order and fluidity are
798 diversely triggered by elicitors of plant defence. JExBot *67*, 5173-5185.
799 47. Cui, Y., Li, X., Yu, M., Li, R., Fan, L., Zhu, Y., and Lin, J. (2018). Sterols regulate endocytic
800 pathways during flg22-induced defense responses in Arabidopsis. Development *145*.
801 48. Blaskovic, S., Blanc, M., and van der Goot, F.G. (2013). What does S-palmitoylation do to
802 membrane proteins? FEBS J *280*, 2766-2774.
803 49. Hurst, C.H., Turnbull, D., Myles, S.M., Leslie, K., Keinath, N.F., and Hemsley, P.A. (2018).
804 Variable Effects of C-Terminal Fusions on FLS2 Function: Not All Epitope Tags Are
805 Created Equal. Plant Physiol *177*, 522-531.
806 50. Zipfel, C., Robatzek, S., Navarro, L., Oakeley, E.J., Jones, J.D., Felix, G., and Boller, T.
807 (2004). Bacterial disease resistance in Arabidopsis through flagellin perception. Nature
808 *428*, 764-767.
809 51. Karimi, M., Inze, D., and Depicker, A. (2002). GATEWAY vectors for Agrobacterium-
810 mediated plant transformation. Trends Plant Sci *7*, 193-195.
811 52. Koncz, C., and Schell, J. (1986). The promoter of TL-DNA gene 5 controls the tissue-
812 specific expression of chimaeric genes carried by a novel type of Agrobacterium binary
813 vector. Mol. Gen. Genet. *204*.
814 53. Kemmerling, B., Schwedt, A., Rodriguez, P., Mazzotta, S., Frank, M., Qamar, S.A.,
815 Mengiste, T., Betsuyaku, S., Parker, J.E., Mussig, C., et al. (2007). The BRI1-associated
816 kinase 1, BAK1, has a brassinolide-independent role in plant cell-death control. Curr Biol
817 *17*, 1116-1122.
818 54. Clough, S.J., and Bent, A.F. (1998). Floral dip: a simplified method for Agrobacterium-
819 mediated transformation of Arabidopsis thaliana. PlantJ *16*, 735-743.
820 55. Turnbull, D., Yang, L., Naqvi, S., Breen, S., Welsh, L., Stephens, J., Morris, J., Boevink,
821 P.C., Hedley, P.E., Zhan, J., et al. (2017). RXLR Effector AVR2 Up-Regulates a
822 Brassinosteroid-Responsive bHLH Transcription Factor to Suppress Immunity. Plant
823 Physiol *174*, 356-369.
824 56. Schwessinger, B., Roux, M., Kadota, Y., Ntoukakis, V., Sklenar, J., Jones, A., and Zipfel, C.
825 (2011). Phosphorylation-dependent differential regulation of plant growth, cell death,
826 and innate immunity by the regulatory receptor-like kinase BAK1. PLoS Genet *7*,
827 e1002046.
828 57. Wathugala, D.L., Hemsley, P.A., Moffat, C.S., Cremelie, P., Knight, M.R., and Knight, H.
829 (2012). The Mediator subunit SFR6/MED16 controls defence gene expression mediated
830 by salicylic acid and jasmonate responsive pathways. New Phytologist *195*, 217-230.
831 58. Schmittgen, T.D., and Livak, K.J. (2008). Analyzing real-time PCR data by the comparative
832 C(T) method. Nat Protoc *3*, 1101-1108.
833 59. Ishiga, Y., Ishiga, T., Uppalapati, S.R., and Mysore, K.S. (2011). Arabidopsis seedling
834 flood-inoculation technique: a rapid and reliable assay for studying plant-bacterial
835 interactions. Plant Methods *7*, 32.

836 60. Hurst, C.H., Turnbull, D., Plain, F., Fuller, W., and Hemsley, P.A. (2017). Maleimide
837 scavenging enhances determination of protein S-palmitoylation state in acyl-exchange
838 methods. Biotechniques *62*, 69-75.
839 61. Gorinski, N., Wojciechowski, D., Guseva, D., Abdel Galil, D., Mueller, F.E., Wirth, A.,
840 Thiemann, S., Zeug, A., Schmidt, S., Zareba-Koziol, M., et al. (2020). DHHC7-mediated
841 palmitoylation of the accessory protein barttin critically regulates the functions of ClC-K
842 chloride channels. JBC *295*, 5970-5983.
843 62. Borner, G.H., Sherrier, D.J., Weimar, T., Michaelson, L.V., Hawkins, N.D., Macaskill, A.,
844 Napier, J.A., Beale, M.H., Lilley, K.S., and Dupree, P. (2005). Analysis of detergent-
845 resistant membranes in Arabidopsis. Evidence for plasma membrane lipid rafts. Plant
846 Physiol *137*, 104-116.
847 63. Martz, F., Wilczynska, M., and Kleczkowski, L.A. (2002). Oligomerization status, with the
848 monomer as active species, defines catalytic efficiency of UDP-glucose
849 pyrophosphorylase. Biochem J *367*, 295-300.
850 64. Gronnier, J., Franck, C.M., Stegmann, M., DeFalco, T.A., Cifuentes, A.A., Dünser, K., Lin,
851 W., Yang, Z., Kleine-Vehn, J., Ringli, C., et al. (2020). FERONIA regulates FLS2 plasma
852 membrane nanoscale dynamics to modulate plant immune signaling. bioRxiv.
853 65. Ershov, D., Phan, M.S., Pylvanainen, J.W., Rigaud, S.U., Le Blanc, L., Charles-Orszag, A.,
854 Conway, J.R.W., Laine, R.F., Roy, N.H., Bonazzi, D., et al. (2022). TrackMate 7: integrating
855 state-of-the-art segmentation algorithms into tracking pipelines. NatMet *19*, 829-832.
856 66. Schindelin, J., Arganda-Carreras, I., Frise, E., Kaynig, V., Longair, M., Pietzsch, T.,
857 Preibisch, S., Rueden, C., Saalfeld, S., Schmid, B., et al. (2012). Fiji: an open-source
858 platform for biological-image analysis. NatMet *9*, 676-682.
859 67. Jaqaman, K., Loerke, D., Mettlen, M., Kuwata, H., Grinstein, S., Schmid, S.L., and
860 Danuser, G. (2008). Robust single-particle tracking in live-cell time-lapse sequences.
861 NatMet *5*, 695-702.
862 68. Parutto, P., Heck, J., Lu, M., Kaminski, C., Avezov, E., Heine, M., and Holcman, D. (2022).
863 High-throughput super-resolution single-particle trajectory analysis reconstructs
864 organelle dynamics and membrane reorganization. Cell Rep Methods *2*, 100277.
865 69. Sage, D., Neumann, F.R., Hediger, F., Gasser, S.M., and Unser, M. (2005). Automatic
866 tracking of individual fluorescence particles: application to the study of chromosome
867 dynamics. IEEE Transactions on Image Processing *14*, 1372-1383.
868 70. Bolte, S., and Cordelieres, F.P. (2006). A guided tour into subcellular colocalization
869 analysis in light microscopy. J Microsc *224*, 213-232.
870 71. Kelley, L.A., Mezulis, S., Yates, C.M., Wass, M.N., and Sternberg, M.J. (2015). The Phyre2
871 web portal for protein modeling, prediction and analysis. Nat Protoc *10*, 845-858.
872 72. Blaum, B.S., Mazzotta, S., Noldeke, E.R., Halter, T., Madlung, J., Kemmerling, B., and
873 Stehle, T. (2014). Structure of the pseudokinase domain of BIR2, a regulator of BAK1-
874 mediated immune signaling in Arabidopsis. J Struct Biol *186*, 112-121.
875 73. Ittisoponpisan, S., Islam, S.A., Khanna, T., Alhuzimi, E., David, A., and Sternberg, M.J.E.
876 (2019). Can Predicted Protein 3D Structures Provide Reliable Insights into whether
877 Missense Variants Are Disease Associated? J Mol Biol *431*, 2197-2212.

878

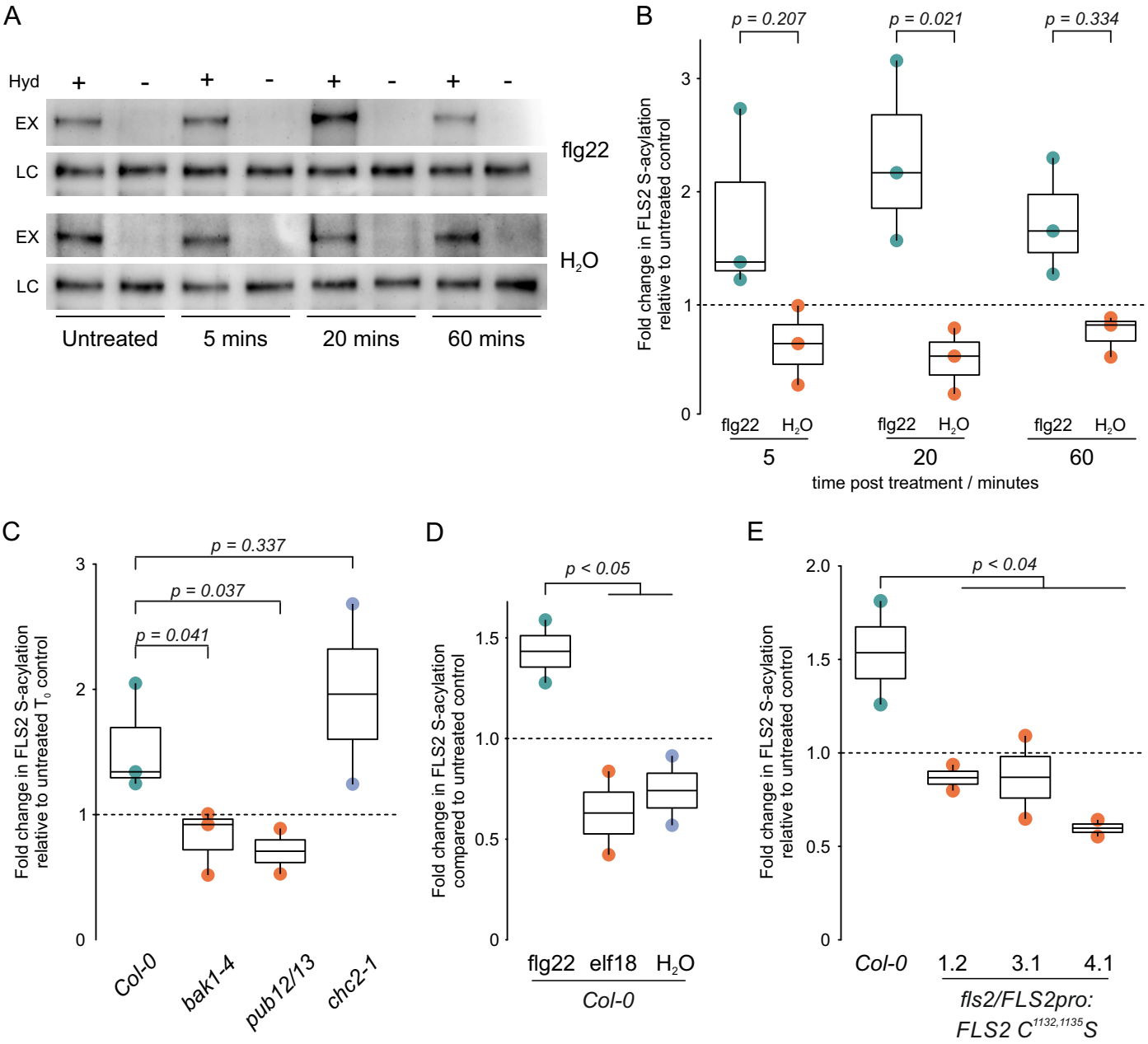

Figure 1. FLS2 S-acylation increases upon flg22 perception. A. Representative western blot of FLS2 S-acylation state in Arabidopsis Col-0 plants treated with 1 μM flg22 peptide or water as determined by acyl-biotin exchange assay**.** EX - indicates S-acylation state, LC - loading control, Hyd - indicates presence (+) or absence (-) of hydroxylamine. **B.** Quantification of western blot data in A. showing change in S-acylation state in Arabidopsis *Col-0* plants treated with 1 μM flg22 (green) or water (orange). S-acylation state is shown relative to untreated plants (black dashed line). n = 3 biological repeats. Box plot shows median and IQR, whiskers indicate data points within 1.5 x IQR. Significance of difference between flg22 and water treatments at each timepoint was determined by ANOVA and Tukey's HSD test. **C.** S-acylation of FLS2 in response to flg22 requires BAK1 and PUB12/13 but not CHC2. S-acylation state was determined by acyl-biotin exchange after 20 minutes exposure to 1 μM flg22 and is shown relative to untreated Arabidopsis plants of the same genotype (dashed line). Box plot shows median and IQR, whiskers indicate data points within 1.5 x IQR. Significant differences of each genotype to flg22 treated Arabidopsis *Col-0* as determined by Student's t-test are shown. **D.** FLS2 undergoes S-acylation in response to flg22 treatment but not elf18. S-acylation state as determined by acyl-biotin exchange after 20 minutes of treatment using 1 μM peptide or water is shown relative to untreated Arabidopsis plants (black, dashed line). Box plot shows median and IQR, whiskers indicate data points within 1.5 x IQR. Significant differences of elf18 or water treatment compared to flg22 treated Arabidopsis *Col-0* as determined by Student's t-test are shown**. E.** FLS2 $C^{1132,1135}S$ mutants are blocked in flg22 mediated increases in S-acylation. S-acylation state is shown following 20 minutes 1 μM flg22 treatment relative to untreated Arabidopsis plants of the same genotype (black, dashed line). Box plot shows median and IQR, whiskers indicate data points within 1.5 x IQR. Significant difference of each line compared to flg22 treated *Col-0* as determined by Student's t-test are shown.

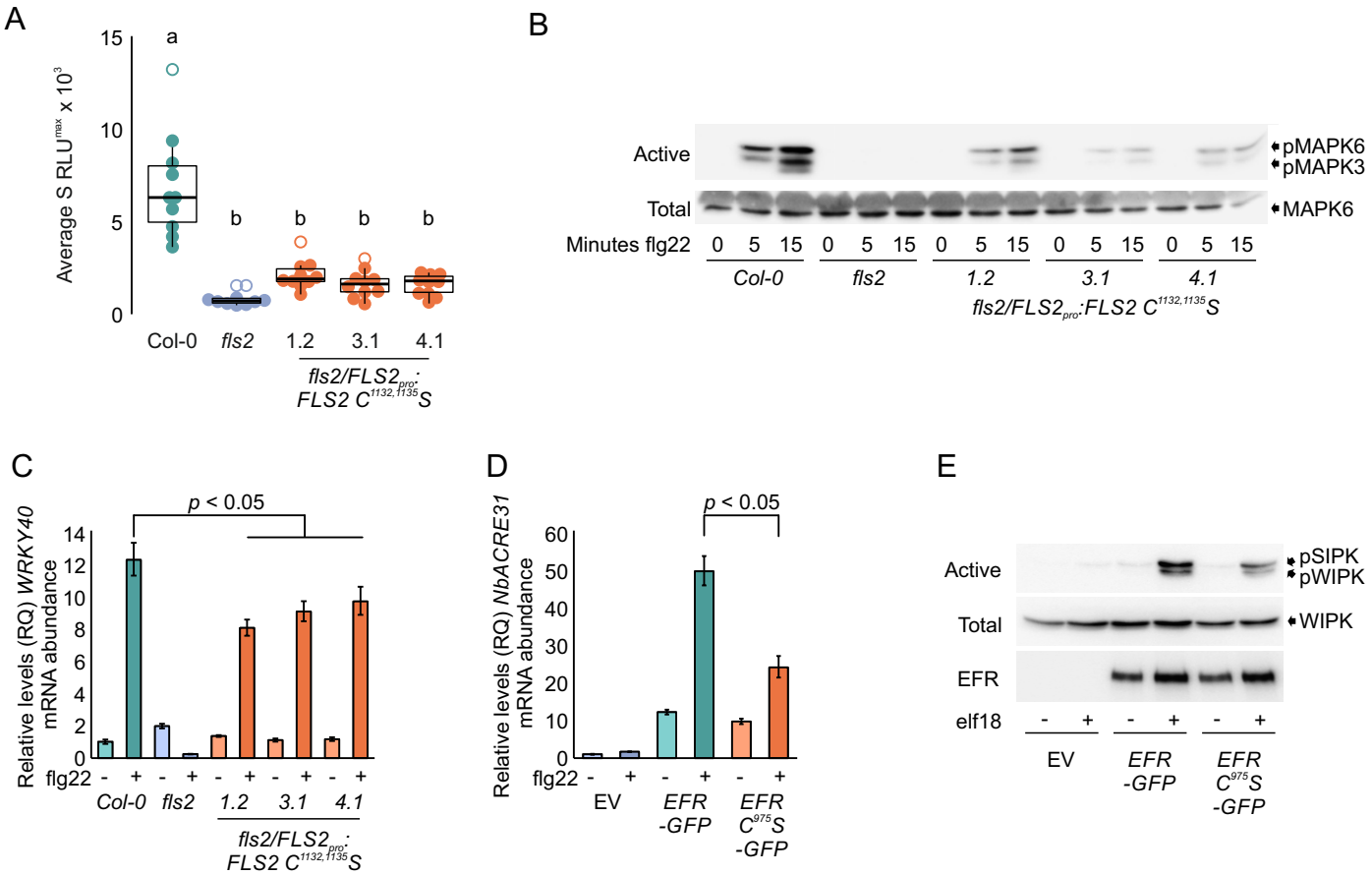

Figure 2. Acute responses to bacterial elicitor perception are reduced in FLS2 C^{1132,1135}S and EFR-C^{975}S expressing plants. A. ROS production induced by 100 nM flg22 treatment of Arabidopsis seedlings. Data points are the sum of the 3 highest consecutive readings per sample. n = 10 per genotype. Statistical outliers are shown as open circles. Box shows median and IQR, whiskers show +/- 1.5 x IQR. Statistically significant differences at $p < 0.01$ are indicated (a, b) and were calculated using ANOVA and Tukey HSD tests. **B**. MAPK activation in *fls2/FLS2pro:FLS2 C^{1132,1135}S* Arabidopsis seedlings in response to 100 nM flg22 as determined over time by immunoblot analysis. pMAPK6/pMAPK3 show levels of active form of each MAPK. MAPK6 indicates total levels of MAPK6 as a loading control. Upper shadow band in MAPK6 blot is RUBISCO detected non-specifically by secondary antibody. **C.** *WRKY40* mRNA abundance after 1 hour treatment with 1 μM flg22 in *fls2/FLS2pro:FLS2 C^{1132,1135}S* Arabidopsis seedlings as determined by qRT-PCR. **D.** *NbACRE31* mRNA abundance after 3 hour treatment with 1 μM elf18 in *EFR-GFP* and *EFR C^{975}S-GFP* expressing *N. benthamiana* plants as determined by qRT-PCR. Values were calculated using the $\Delta\Delta C_T$ method, error bars represent RQ_{MIN} and RQ_{MAX} and constitute the acceptable error level for a 95% confidence interval according to Student's t-test. **E.** MAPK activation in *EFR-GFP and EFR C^{975}S*-GFP expressing *N. benthamiana* plants in response to 15 minutes treatment with 1 μM elf18 as determined by immunoblot analysis. pSIPK/pWIPK show levels of active form of each MAPK. WIPK indicates total levels of WIPK as a loading control. EFR-GFP and EFR C^{975}S-GFP levels are shown as a control for dosage effects on MAPK activation.

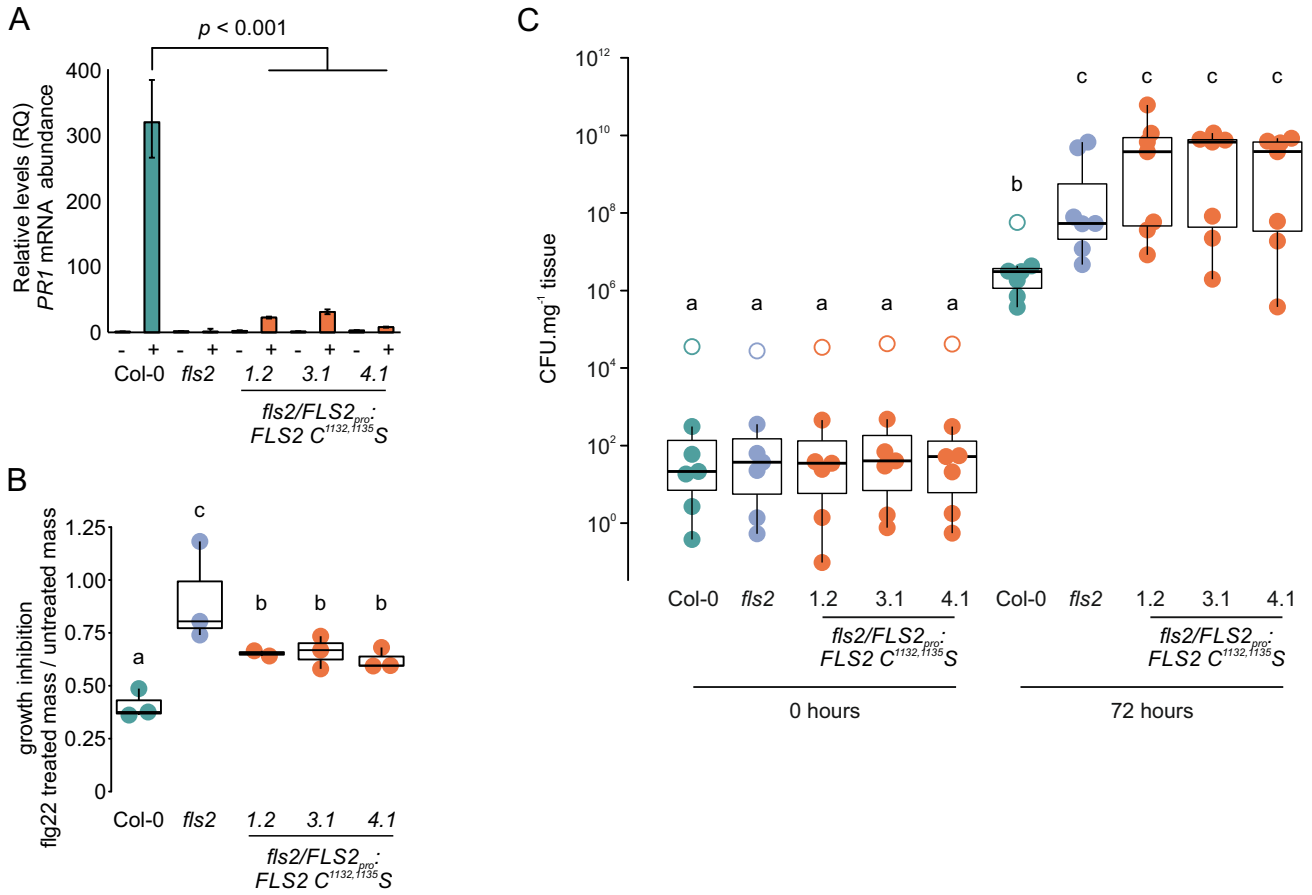

Figure 3. FLS2 S-acylation is required for long term immune response outputs (A). Induction of *PR1* gene expression after 24 hours treatment with 1 μM flg22 in *fls2/FLS2pro:FLS2 C*^{1132,1135}*S* seedlings as determined by qRT-PCR. Values were calculated using the $\Delta\Delta C_T$ method, error bars represent RQ_{MIN} and RQ_{MAX} and constitute the acceptable error level for a 95% confidence interval according to Student's t-test. Significant differences in transcript mRNA detected in *fls2/FLS2pro:FLS2 C*^{1132,1135}*S* Arabidopsis seedlings compared to Col-0 levels in flg22 treated samples are indicated. Similar data were obtained over 3 biological repeats. **(B).** Inhibition of growth after 10 days of 1 μM flg22 treatment is reduced in *fls2/FLS2pro:FLS2 C*^{1132,1135}*S* Arabidopsis seedlings. Box and whisker plots show data from 3 biological repeats (box denotes median and IQR, whiskers show +/- 1.5 x IQR), significant differences at $p < 0.01$ are indicated (a, b, c) and calculated by ANOVA with Tukey HSD test **(C).** Resistance to *P. syringae* DC3000 infection is impaired by loss of FLS2 S-acylation in fls2/FLS2pro:FLS2 C^{1132,1135}S Arabidopsis plants. Box and whisker plots show data from 7 biological repeats (box denotes median and IQR, whiskers show +/- 1.5 x IQR, outliers are shown as open circles), significant differences at $p < 0.05$ are indicated (a, b, c) and calculated by ANOVA with Tukey HSD test.

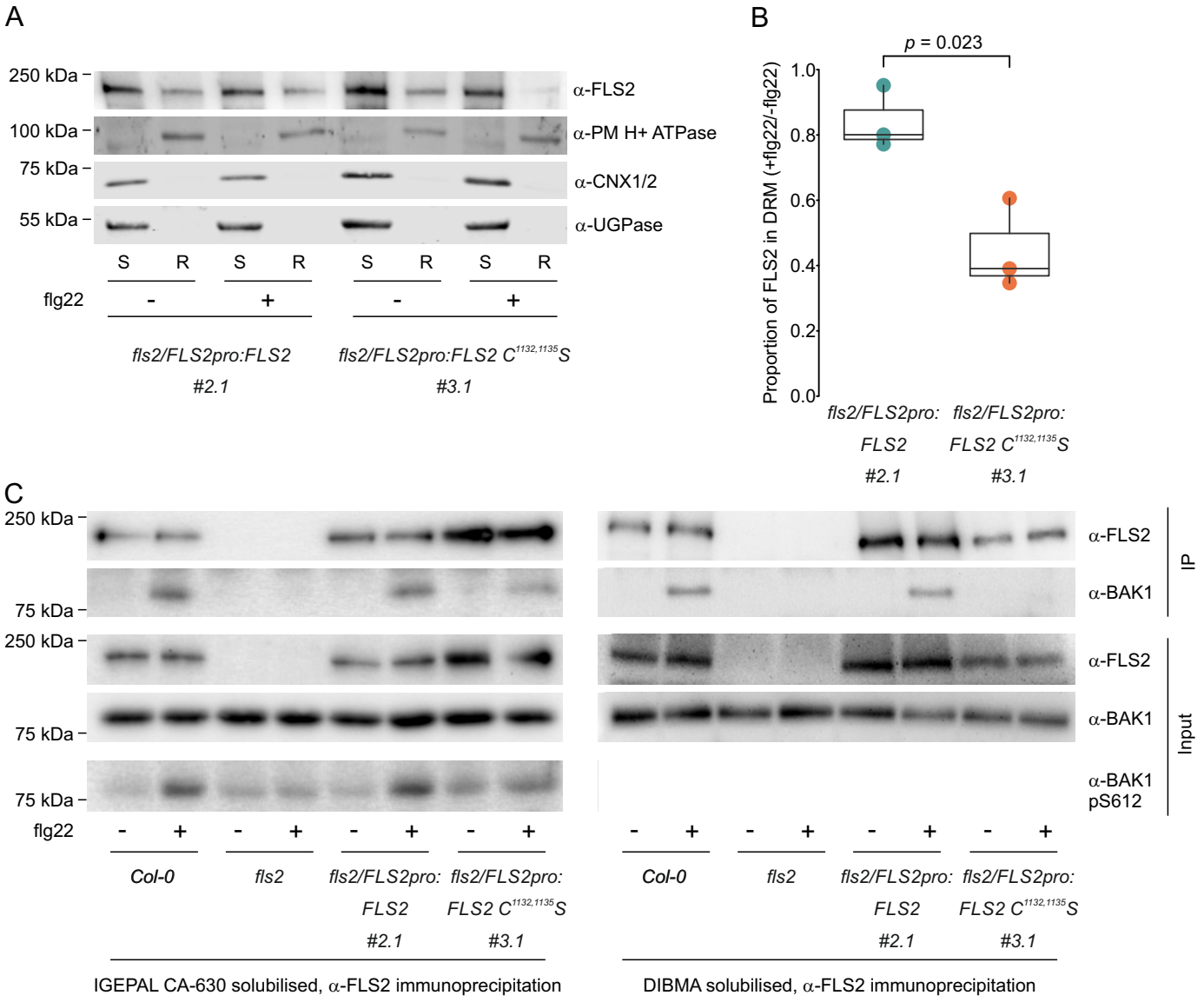

Figure 4. FLS2 $C^{1132,1135}S$ shows reduced interaction with BAK1 following flg22 stimulation. A. FLS2 $C^{1132,1135}S$ shown altererd DRM partitioning compared to FLS2. Arabidopsis flg22 treated seedlings were lysed in cold IGEPAL CA-630 buffer and separated into detergent soluble (S) and detergent resistant (R) fractions. Relative partitioning of FLS2 into each fraction was determined by western blotting with anti-FLS2 rabbit polyclonal antibody. Purity of fractions is shown by western blot using anti-PM H+ ATPase (PM ATPase, DRM marker), anti-Calnexin1/2 (CNX1/2, DSM marker) and anti-UDP-glucose pyrophosphorylase (UGPase, cytosol marker) antibodies. **B.** Quantification of FLS2 data shown in A. from 3 biological repeats. Box plot shows median and IQR, whiskers indicate data points within 1.5 x IQR. Significance was calculated using Student's t-test. **C.** FLS2 was immunoprecipitated from IGEPAL CA-630 (left) or DIBMA (right) solubilised flg22 treated Arabidopsis seedling lysates using anti-FLS2 rabbit polyclonal antibody. BAK1 recovery was assessed using rabbit polyclonal anti-BAK1 antibody. flg22 induced BAK1 autophosphorylation at Ser612 was assessed in IGEPAL CA-630 solubilised input samples using rabbit polyclonal anti-BAK1 pS612 antibody.

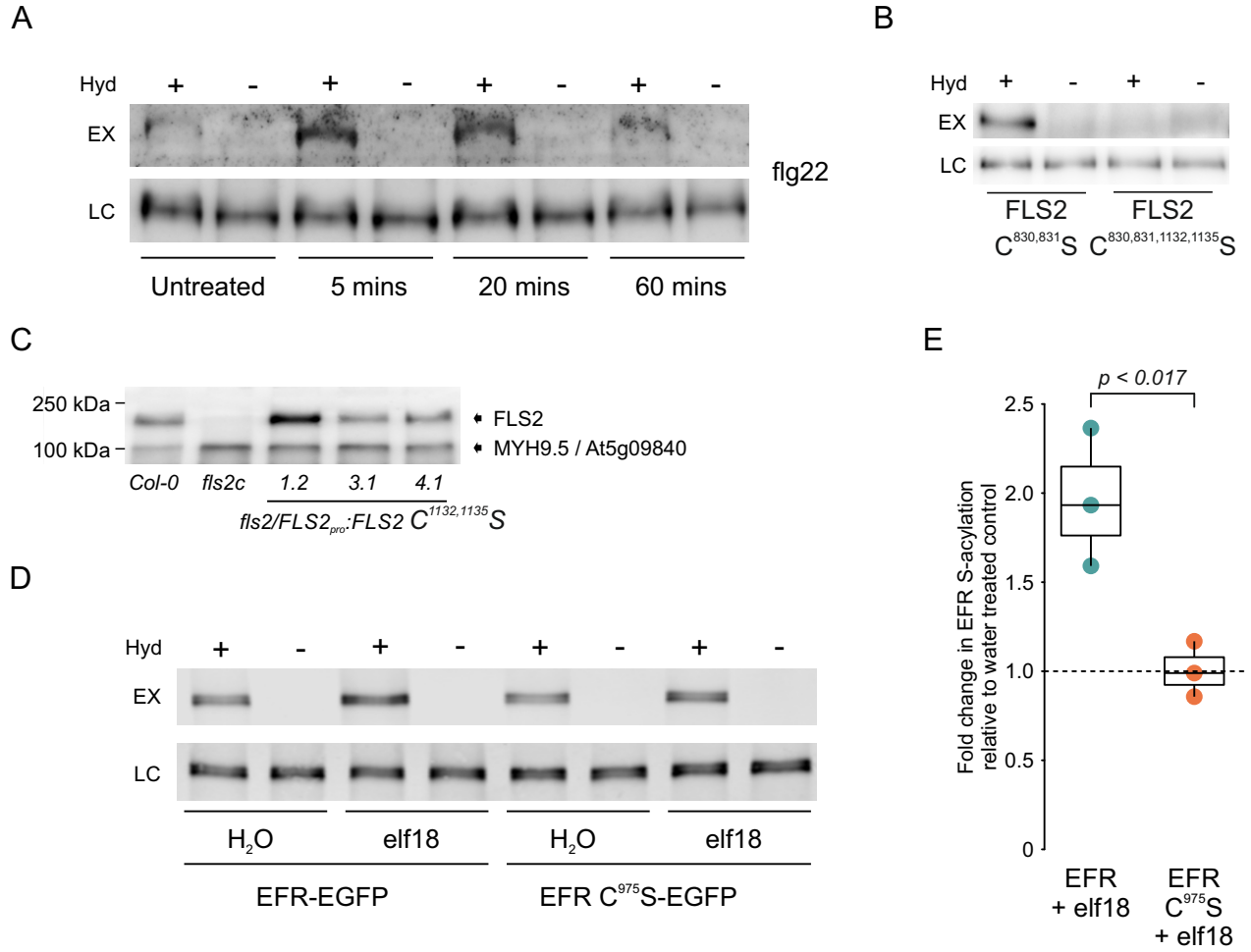

Supplemental figure 1. A. FLS2 $C^{830,831}S$ stably expressed in Arabidopsis *fls2* null mutant background retains the ability to be weakly S-acylated following flg22 treatment. S-acylation state was determined by acyl-biotin exchange assay. EX - indicates S-acylation state, LC - loading control, Hyd - indicates presence (+) or absence (-) of hydroxylamine. **B.** Mutation of FLS2 Cys1132,1135 to serine abolishes residual S-acylation observed in FLS2 $C^{830,831}S$ when over-expressed in *Nicotiana benthamiana.* EX - indicates S-acylation state, LC - loading control, Hyd - indicates presence (+) or absence (-) of hydroxylamine. **C.** Expression levels of FLS2 $C^{1132,1135}S$ in *fls2/FLS2$_{pro}$:FLS2 FLS2 $C^{1132,1135}S$* transgenic Arabidopsis lines used in this study. 50 mg total protein from 7 day old seedlings was loaded per lane. MYH9.5 / At5g09840 is a previously reported cross-reacting protein with the primary anti-FLS2 antibody used . **D.** EFR-GFP expressed in *N. benthamiana* undergoes S-acylation in a Cys975 dependant manner after 20 minutes of 1 μM elf18 treatment. S-acylation state was determined by determined by acyl-biotin exchange assay. EX - indicates S-acylation state, LC - loading control, Hyd - indicates presence (+) or absence (-) of hydroxylamine. **E.** Quantification of EFR S-acylation state shown in D. elf18 induced changes to S-acylation state are shown relative to water treated (black dashed line). n = 3 biological repeats. Box plot shows median and IQR, whiskers indicate data points within 1.5 x IQR. Significance of difference between EFR and EFR C975S was determined by Student's t-test.

```
At5g46330 FLS2              1125 IEDFLKLCLFCTSSRPEDRPDMNEILTHLM 1154
At5g20480 EFR                965 LRLVLQVGIKCSEEYPRDRMRTDEAVRELI 994
At3g24550 AtPERK1            525 MARMVACAAACVRHSARRRPRMSQIVRALE 554
At2g48010 RKF3               529 LEKYVLIAVLCSHPQLHARPTMDQVVKMLE 558
At3g51550 FERONIA            779 FKKFAETAMKCVLDQGIERPSMGDVLWNLE 808
Cb A0A388L3P2 CrRLK          968 LYKVAEVALRCLGEDRDTRPSMTDVRRGLE 997
At1g18390 AtLRK10L-1.2       582 VIAVAELAFQCLQSDKDLRPCMSHVQDTLT 611
At2g20300 AtALE2             588 MAKVAAIASMCVHQEVSHRPFMGEVVQALK 617
At1g52310 C-lec RLK          514 VQKVVDLVYSCTQNVPSMRPRMSHVVHQLQ 543
Kn A0A1Y1HV38 C-lec RLK      718 AFTVAYLIAQCLAELPEDRPSMSTVVTGLK 747
At3g26700 RLCK-IXa           320 VEELITLTLRCVDVSSEKRPTMSFVVTELE 349
At1g21250 WAK1               651 IQEAARIAAECTRLMGEERPRMKEVAAKLE 680
At5g38280 AtPR5K1            577 AKKLVLVALWCIQMNPSDRPPMIKVIEMLE 606
At5g60300 AtP2K1             584 VEMVMKLGLLCSNIVPESRPTMEQVVLYLN 613
At1g19090 AtCRK1             543 ALKVLQIGLLCVQSSVELRPSMSEIVFMLQ 572
At1g11330 G-lec RLK          765 IEKCVHIGLLCVQEVANDRPNVSNVIWMLT 794
At3g59420 AtCR4              567 LKRIVSVACKCVRMRGKDRPSMDKVTTALE 596
At3g21630 AtLYK1 LysM RLK    562 VYKMAELGKACTQENAQLRPSMRYIVVALS 591
Cb A0A388KNI4 LysM RLK      1226 VIKMAEVAVRCVQENPEARPDMKRVAYELD 1255
consensus                        ----------C-------RP----------
```

Supplemental figure 2. Receptor Kinases contain a conserved C-terminal cysteine within the kinase domain. Alignment using at least one representative member from each of the wider Arabidopsis RK superfamilies. Example receptor kinases found in *Chara braunii* (Cb) and *Klebsormidium nitens* (Kn) with clear sub-family members in Arabidopsis are also included as extant basal Streptophytes to illustrate evolutionary conservation of the proposed S-acylation site. Uniprot IDs are given for *Chara* and *Klebsormidium* sequences. Aligment is centred on the conserved C$[X]_7$RP motif (orange) found in the loop between the G- and H-helices of the kinase domain. Putative S-acylation site cysteines are highlighted in teal with the conserved +7 RP motif in orange.

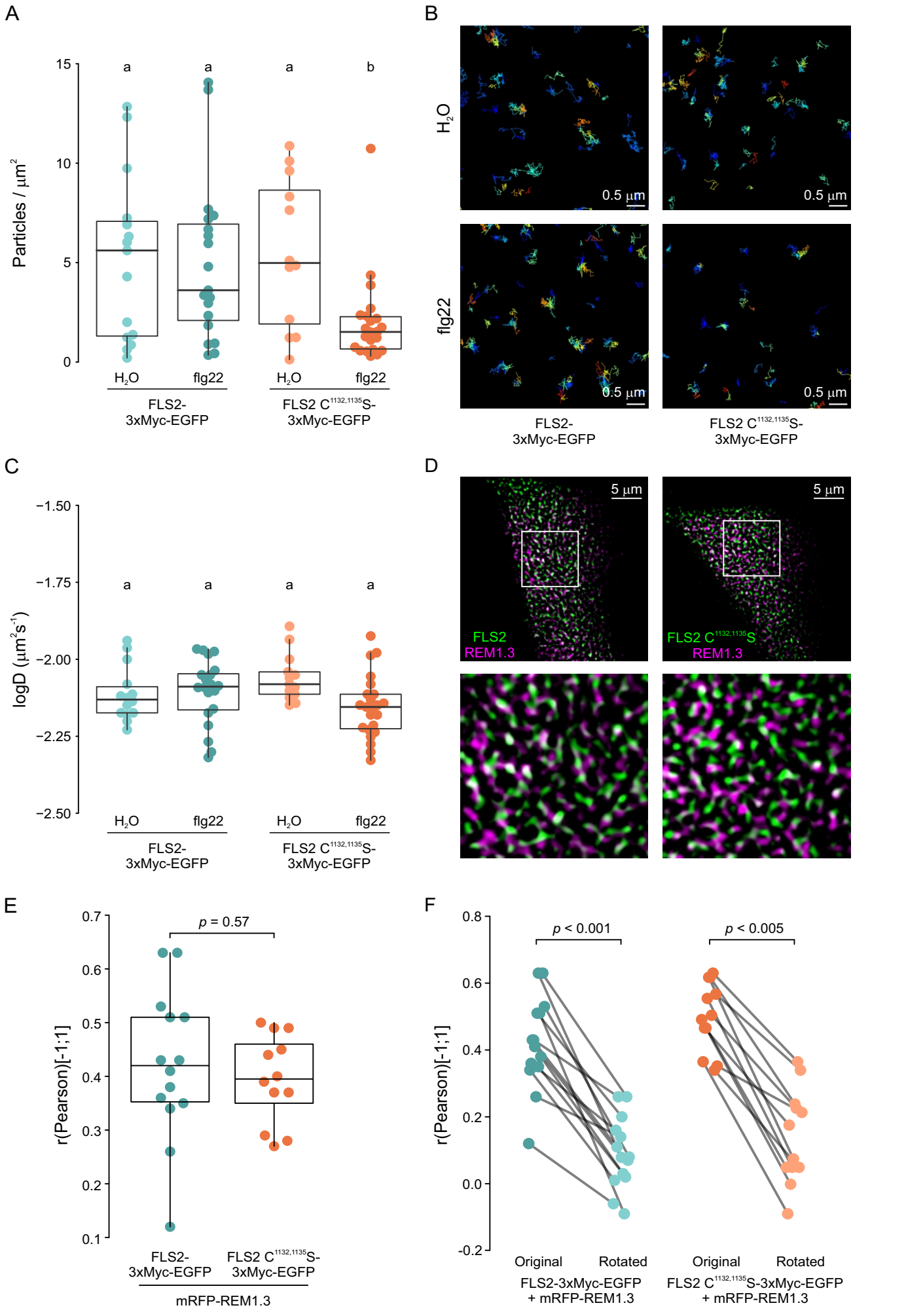

Supplemental figure 3. FLS2 S-acylation affects flg22 induced endocytosis but not unstimulated basal behaviour. A. FLS2-3xMyc-GFP and FLS2 $C^{1132,1135}$S-3xMyc-GFP accumulate similarly when expressed in *N. benthamiana* in the absence of flg22, however, FLS2 $C^{1132,1135}$S-3xMyc-GFP is cleared more rapidly from the cell surface following flg22 exposure than FLS2-3xMyc-GFP. Particle counts per μm^2 at the plasma membrane of single cells using TIRF microscopy. Box plot shows median and IQR, whiskers indicate data points within 1.5 x IQR. FLS2-3xMyc-GFP mock n = 15 cells and 15076 particles, FLS2-3xMyc-GFP flg22 treatment n = 19 cells and 14717 particles, FLS2 $C^{1132,1135}$S-3xMyc-GFP mock n = 12 cells and 12593 particles and FLS2 $C^{1132,1135}$S-3xMyc-GFP flg22 treatment n= 22 cells and 7468 particles. *p* values calculated by ANOVA and confidence groups at $p < 0.05$ assigned using Tukey's HSD test. **B.** Representative images from single particle tracking experiments of FLS2-3xMyc-GFP and FLS2 $C^{1132,1135}$S-3xMyc-GFP at the plasma membrane using TIRF microscopy used to generate graph in A. Experiments were performed transiently in *N. benthamiana.* **C.** Quantification of data in B. Box plot shows median and IQR, whiskers indicate 1.5 x IQR. *p* values calculated by ANOVA and confidence groups at $p < 0.05$ assigned using Tukey's HSD test. **D.** FLS2-3xMyc-GFP and FLS2 $C^{1132,1135}$S-3xMyc-GFP form nanodomains in the plasma membrane and show similar co-localisation with mRFP-REM1.3 nanodomains when transiently expressed in *N. benthamiana* in the absence of flg22. Representative micrographs of FLS2-3xMyc-GFP and FLS2 $C^{1132,1135}$S-3xMyc-GFP (green) co-localisation with mRFP-REM1.3 (magenta) at the plasma membrane of single epidermal cells using TIRF microscopy. **E.** Quantification of FLS2-3xMyc-GFP or FLS2 $C^{1132,1135}$S-3xMyc-GFP co-localisation with mRFP-REM1.3 at the plasma membrane of single epidermal cells. FLS2-3xMyc-GFP n = 14, FLS2 $C^{1132,1135}$S-3xMyc-GFP n = 12**.** Box plot shows median and IQR, whiskers indicate 1.5 x IQR. *p* value calculated using Student's t-test. **F.** To determine whether measured co-localisation values shown in B (original) were significant, co-localisation analysis was repeated after rotation of the mRFP-REM1.3 image by 90 degrees (rotated). In all cases, co-localisation was reduced and overall significantly different, indicating that the co-localisation observed in B is both specific and significant. *p* values were calculated using Student's t-test.

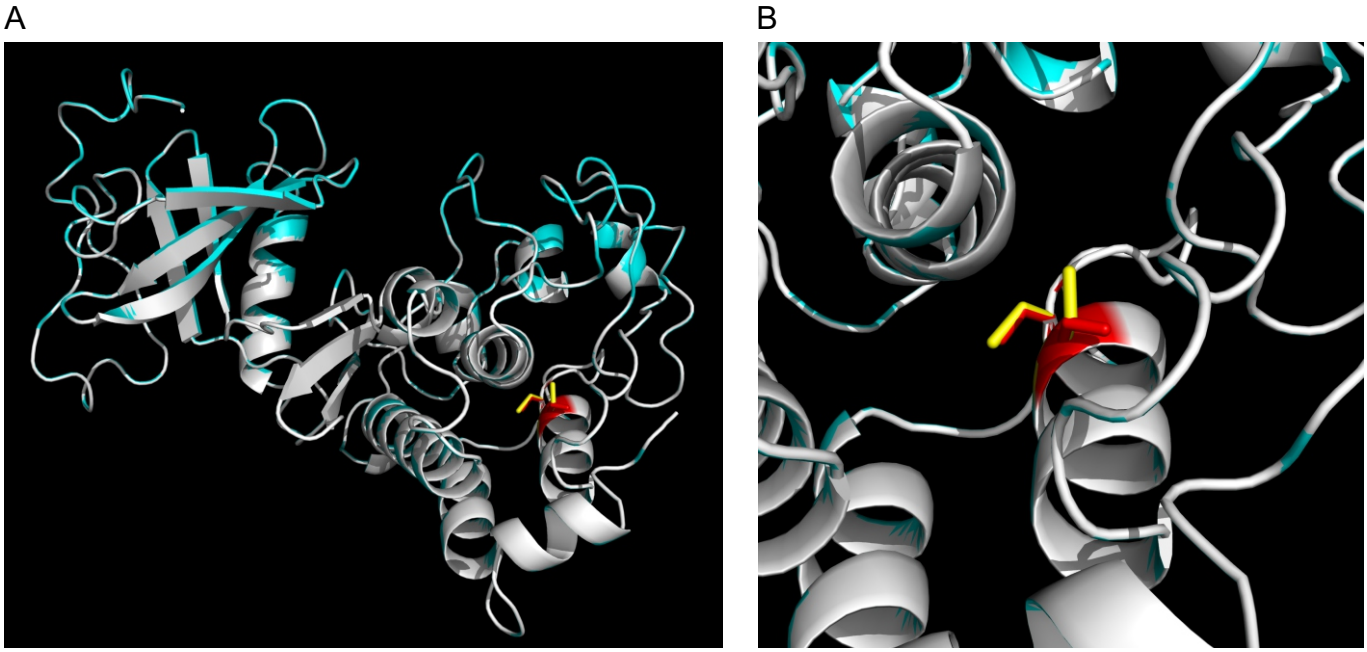

Supplemental figure 4. Mutation of kinase domain S-acylation site cysteines to serine in FLS2 is not predicted to affect kinase domain structure. A. Superimposition of the modelled structures of FLS2 (white) and FLS2 $C^{1132,1135}S$ (blue) kinase domains. **B.** Zoomed in view of Cys1132,1135 in FLS2 (yellow) and substituted serine (red) residues in FLS2 $C^{1132,1135}S$. Only the proton of Ser1132 is predicted to diverge from the FLS2 structure, being rotated by ~110 degrees compared to the original cysteine. This rotation does not affect the position or packing of any other amino acid.